2013

Metrology Of Volume Chirped Bragg Gratings Recorded In Photo-thermo-refractive Glass For Ultrashort Pulse Stretching And Compressing

Christopher Lantigua
University of Central Florida

METROLOGY OF VOLUME CHIRPED BRAGG GRATINGS RECORDED IN PHOTO-THERMO-REFRACTIVE GLASS FOR ULTRASHORT PULSE STRETCHING AND COMPRESSING

by

CHRISTOPHER A. LANTIGUA
B.S. University of Florida 2010

A thesis submitted in partial fulfillment of the requirements
for the degree of Master of Science
in the College of Optics & Photonics
at the University of Central Florida
Orlando, Florida

Summer Term
2013

Major Professor: Leonid B. Glebov

ABSTRACT

Chirped Bragg gratings (CBGs) recorded in photo-thermo-refractive (PTR) glass provide a very efficient and robust way to stretch and compress ultra-short laser pulses. These gratings offer the ability to stretch pulses from hundreds of femtoseconds, to the order of 1 ns and then re-compress them. However, in order to achieve pulse stretching of this magnitude, 100 mm thick CBGs are needed. Using these CBGs to both stretch, and re-compress the pulse thus requires propagation through 200 mm of optical glass. This therefore demands perfect control of the glass homogeneity, as well as the holographic recording process of the CBG.

In this thesis, we present a study of the CBG parameters that lead to distortions in the quality of diffracted beams. We first present the challenges associated with measuring the quality of these beams and we show that such measurements are not easily achieved using commercial systems that rely on the ISO standard M^2 method. Thus, we introduce a new metric of beam quality, which we have coined S^2, that is a combination of both the M^2 and power in the bucket metrics. Subsequently, we investigate the influence of the CBG parameters on the quality of diffracted beams. In particular, we examine the impact of small optical heterogeneities known as striae, as well as the impact of the optically and thermally induced distortions in the grating. We then use this data to improve the fabrication and characterization of 100 mm long CBGs.

Finally, we characterize the performance of CBGs recorded in PTR for stretching and compression of femtosecond pulses using a custom autocorrelation system. We present data on high quality 100 mm long CBGs and an analysis on the correlation between beam quality and the final pulse duration after stretching and re-compressing the pulse.

To my mother and father:
For without whom, none of this is possible.

ACKNOWLEDGMENTS

I would like to thank my advisor Dr. Leonid B. Glebov, for providing me the opportunity to perform this research. When I started at CREOL I had little experience in optics, but you took a chance on me and allowed me to grow. Your stories and historical perspective will always be remembered.

I would like to thank my committee members Dr. Axel Shulzgen and Dr. Boris Zeldovich for their constructive remarks on my thesis, as well as for sharing their knowledge of optics.

Thank you to Vadim Smirnov and the Optigrate Corporation for providing the CBGs for this work.

A special thanks to Dr. Julien Lumeau, who has been a mentor and a friend to me. Thank you for all your knowledge, your patience and guidance throughout these years, for helping me to grow not only in optics, but as a researcher and a scientist. I have learned so much from you my friend and I want to say thank you.

Thanks to the PPL team past and present: Brian Anderson, Daniel Ott, Marc Segall, Sergiy Mokhov, Ivan Divanlasky, and George Venus.

I would like to thank all my family for all their support. Sarah, Mima, Nana, Abuelo… thank you all. Especially my mother and my father, whose sacrifices and dedication as parents have allowed me to get where I am today.

Finally, I would like thank Lynette, a very special girl who has been by my side every step of the way. Thank you for always being so supportive and patient, for always listening to all my science talk. I can’t thank you enough.

TABLE OF CONTENTS

LIST OF FIGURES

LIST OF TABLES

LIST OF NOMENCLATURE

BBP	Beam Parameter Product
BQ	Beam Quality
CBG	Chirped Bragg Grating
COM	Center of Mass
CPA	Chirped Pulse Amplifcation
GRIN	Gradient of Refractive Index
GVD	Group Velocity Dispersion
PIB	Power in the Bucket
PTR	Photo-Thermo-Refractive Glass
USP	Ultra-Short Pulse
VBG	Volume Bragg Grating
cm	Centimeter (10^{-2} m)
mm	Millimeter (10^{-3} m)
μm	Micrometer (10^{-6} m)
nm	Nanometer (10^{-9} m)
ppm	Parts per million (10^{-6})
mW	Milliwatt (10^{-3} W)
ns	Nanosecond (10^{-9} s)
ps	Picosecond (10^{-12} s)
fs	Femtosecond (10^{-15} s)

CHAPTER ONE: INTRODUCTION TO PTR GLASS AND CHIRPED BRAGG GRATINGS

The demand for high power laser systems operating at near infrared wavelengths is continuously increasing as these laser sources are finding more applications in telecommunications, range finding, remote sensing… As a result, there has been an accompanying increase in demand for optical elements capable of withstanding the high-energy imposed by such lasers. Volume Bragg gratings (VBGs) offer a unique solution for such high-energy laser systems. These elements are high efficiency phase volume holograms recorded in optical quality silicate glass: photo-thermo-refractive (PTR) glass. Its low absorption and scattering makes it ideal for high power and high-energy laser systems. Transmitting, reflecting, and chirped Bragg gratings have all been demonstrated in PTR glass [1.1], and with diffraction efficiencies > 95% [1.2]. The technology for developing volume Bragg gratings in PTR glass has matured, making these gratings commercially available [1.3].

Of particular interest in this thesis, chirped Bragg gratings (CBGs) recorded in PTR glass can be used to both stretch and re-compress femtosecond and picosecond laser pulses [1.4]. This is especially useful in chirped pulse amplification (CPA) systems, a state of the art technique that allows for generation of pulses with peak powers > 1000 terawatts [1.5]. However, using a CBG both as a stretcher and compressor inside a CPA system requires propagation through the thickness of the grating twice, thus the strictest standards are required for the fabrication of these CBGs, and in general all VBGs, to ensure distortion free beam propagation.

1.1 PTR Glass and VBGs

Photo-thermo-refractive (PTR) glass is a photosensitive, multicomponent silicate glass, doped with fluorine, bromine, cerium, and silver. It has a broad transparency range from 350 to 2700 nm (Fig. 1) and allows for a refractive index change as high as 10^{-3} (1000 ppm) between regions of the glass that have been exposed to UV radiation and regions which remain unexposed [1.6].

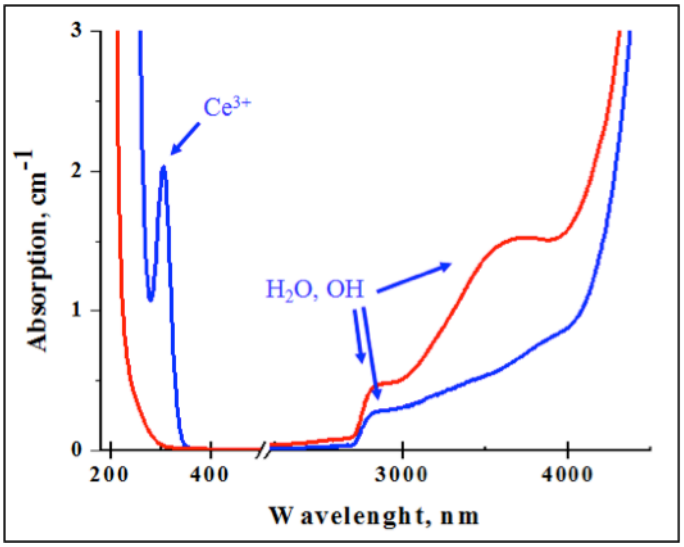

Figure 1: Typical absorption spectrum of PTR glass (in blue) and PTR glass matrix (in red), i.e. without all dopants.

The photosensitivity of PTR glass is derived from a photo-thermal crystallization that was first discovered in silicate glass exposed to UV radiation in the late 1940's by S.D. Stookey [1.7]. The photo-thermal process that gives rise to a permanent change of refractive index [1.6] is based on precipitation of dielectric microcrystals in the bulk glass exposed to UV radiation and is

achieved in a two-step process consisting of, exposure of a PTR sample to UV radiation, followed by thermal development of the sample.

Exposure to UV radiation causes cerium to ionize, thus giving off an electron. Silver cations throughout the glass matrix accept these electrons released from cerium, forming neutral silver containing particles [1.8, 1.9]. At this stage only a latent image has been formed inside the glass and no change of refractive index has occurred. To induce this refractive index change, the sample is developed by heat-treating the glass at a temperature above the glass transition temperature.

The thermal treatment process occurs in two stages. In the first, the glass is heated to 450-500°C causing diffusion of silver atoms. Allowing the sample to rest at this elevated temperature, the diffusion of silver atoms leads to the formation of silver containing clusters in the exposed region of the glass. These silver particles act as nucleation centers for sodium fluoride crystallization.

In stage two of the thermal process, the sample is brought to 500-550°C, at which point cubic sodium fluoride (NaF) crystal growth occurs [1.10]. Cooling of the glass sample down to the room temperature induces stresses caused by the difference in the thermal expansion coefficients of NaF and PTR glass, which induce a refractive index decrement of about 10^{-3} in exposed regions through the photo-elastic properties of the glass [1.11]. This small refractive index change is enough to produce a diffractive optical element in samples with thicknesses more than several hundred micrometers. A summary of this photo-thermal process is shown below in (Fig.2).

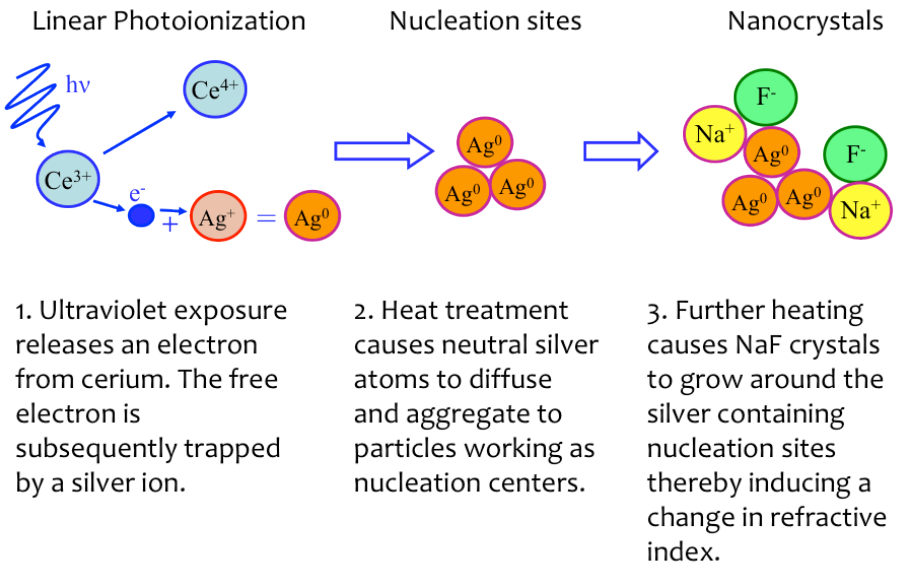

Figure 2: Summary of the photo-thermal process that is at the origin of the photo-thermo-induced refractive index change in PTR glass.

The main application of photo-thermo-refractive glass is the fabrication of volume Bragg gratings and volume phase masks [1.12]. Volume Bragg gratings are fabricated by holographic recording of a sinusoidal refractive index modulation inside the photosensitive medium. Volume Bragg gratings can be categorized into two categories, transmitting and reflecting. For transmitting Bragg gratings (TBGs), the diffracted beam is on the same side as the transmitted beam, while for reflecting Bragg gratings (RBGs) the diffracted beam is on the same side as the incident beam (Fig.3).

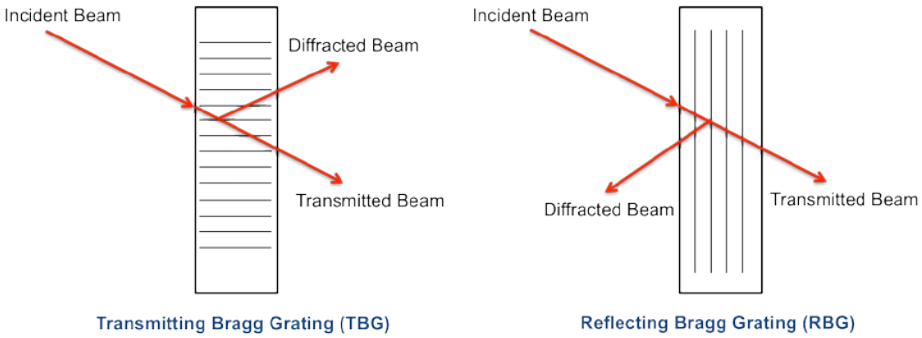

Figure 3: Transmitting and reflecting geometries of volume Bragg gratings.

The high spectral and angular selectivity offered by these elements allow them to be inserted into a variety of laser systems. For example, VBGs have been used for transverse and longitudinal mode selection in laser cavities [1.13, 1.14], they have also been used for spectral beam combining of high power fiber lasers [1.15, 1.16].

Recent advancements in the fabrication and exposure/thermal treatment procedures of PTR glass and VBGs have allowed decreasing the overall losses of PTR glass. Absorption can be as low as $10^{-4}cm^{-1}$, while scattering losses can be kept within $10^{-3}cm^{-1}$ [1.17, 1.18]. Such improvements allow VBGs to be used in high-energy laser systems with powers up to several tens of kilowatts [1.17, 1.19], making them ideal candidates for ultra-short pulse laser systems, in particular for stretching and compressing of femtosecond systems.

1.2 Ultra-short Pulse Lasers, CPA Systems and Chirped Bragg Gratings

The need for high-power, ultra-short pulse lasers continues to grow, as these lasers find more applications amongst a wide range of disciplines in modern science. However, one of the major roadblocks in developing higher power ultra-short pulse lasers is that direct optical

amplification of low-power ultra-short pulses results in detrimental nonlinear effects and laser-induced damage of the amplifying medium due to the extremely high peak powers of amplified pulses. In order to amplify an ultra-short laser pulse, a technique known as chirped pulse amplification (CPA) was developed [1.20].

Chirped pulse amplification is a promising technology enabling the highest average power and pulse energy for ultra-short pulse lasers [1.21]. In a CPA system, ultra-short pulses are stretched temporally by a dispersive optical element before amplification, reducing the peak power of the pulses in the amplifier to a moderate level, so as to not damage the material. Following amplification, the pulses are then temporally re-compressed, again with a dispersive optical element, resulting in stunningly high peak powers (Fig.4).

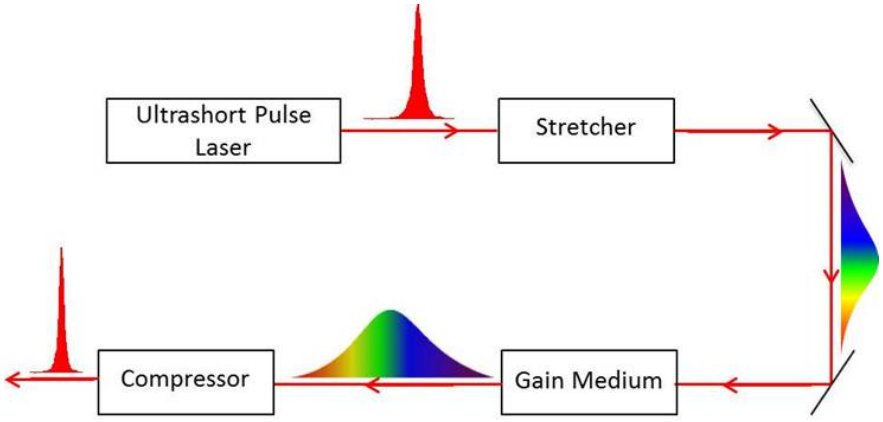

Figure 4: CPA system for amplifying ultra-short laser pulses using a dispersive optical element to temporally stretch the pulse, amplifying the pulse and then using again a dispersive optical element to recompress the pulse.

Clearly, the dispersive optical element used to recompress the pulses must have a high damage threshold. Traditionally, pulse stretching and compressing in CPA systems has been

performed with surface diffraction gratings typically coated with metal [1.21]. However, the relatively low damage threshold of metal-coated gratings limits the average power of such laser systems.

Design of CPA laser systems saw a breakthrough with the development of fiber Bragg gratings (FBGs). Chirped Bragg gratings fabricated inside a fiber replaced pairs of bulky surface gratings as stretchers and compressors [1.22, 1.23]. This approach has dramatically increased the robustness of CPA systems and the inherent compactness of the fiber has enabled their use in harsher environment, not just laboratories. However, a major drawback of fiber Bragg gratings as a compressor is the maximum aperture is limited by the size of the core, thus limiting the ability for further power scaling of fiber CPA systems, as any increased power distributed over the small core area damages the fiber.

Chirped Bragg gratings (CBGs) recorded in photo-thermo-refractive (PTR) glass have changed dramatically the design of high power femtosecond lasers (Fig.5). Replacing bulky pairs of conventional surface gratings in CPA systems, with compact and robust CBGs has enabled a decrease in the size and weight of these systems by several orders [1.24].

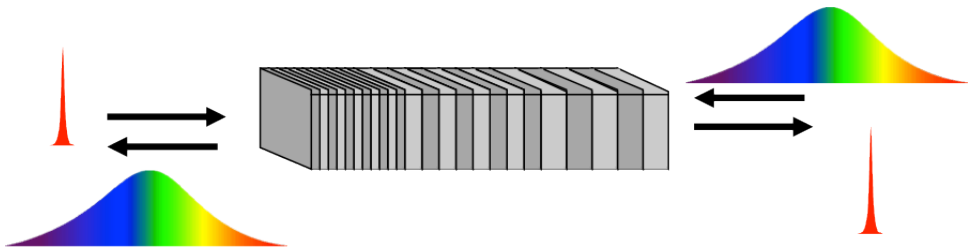

Figure 5: Chirped Bragg grating (CBG) with a variable period along the beam propagation. Grating period and thickness are not in scale; thickness is usually tens of thousand times larger than the period.

A CBG is similar to a fiber Bragg grating, in that a linear variation of the grating period along direction of beam propagation is recorded inside the glass, but unlike the FBG, the CBG is not limited in its ability to be scaled to higher powers due its aperture dimensions. However, conventional CBGs (monolithic, single-pass, retroreflecting) have some limitations determined by the refractive index modulation and losses (scattering and absorption) in PTR glass. These limitations restrain generation of extremely short, high-energy pulses with controllable temporal and/or spectral shape.

One of the main goals of this thesis was to enable a substantial increase in the pulse stretching time achieved by a CBG recorded in PTR, in order to allow for further amplification of pulses and therefore achieve higher intensity after re-compression. Thus, the technical problem to be solved for achieving of the announced goal is increasing the thickness of CBGs without deterioration of beam quality in the stretched and compressed beams. However, a considerable increase of thickness and/or bandwidth of CBGs in PTR glass are beyond available technology of glass fabrication and CBG recording. We thus conducted the study in two directions: the first one is the understanding of the sources of distortions in the beams diffracted by CBGs in order to control or mitigate them, the second is the understanding of multipass stretching and compressing in CBGs, which increases the effective optical path of the CBG (Fig. 6), and will result in the equivalent of a CBG with twice its thickness.

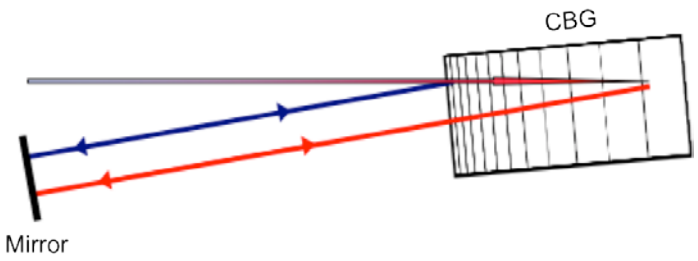

Figure 6: Multipass configuration for double stretching and compression with a CBG.

1.3 Fabrication of Chirped Bragg Gratings

Volume Bragg gratings in PTR glass are recorded by exposure to UV-radiation from a He-Cd laser at 325 nm. Recording any grating inside PTR requires exposing the sample to an interference pattern generated between two UV beams [1.25]. To record a grating with constant period, the typical optical set-up is the following. A He-Cd beam is expanded using a set of beam expanders and beam shapers. A collimated flat-top beam with a diameter up to 100+ mm can be achieved depending on the size of the VBG to be recorded. This large aperture beam is then sent to a 50:50 beam-splitter and the two emerging beams are then redirected to the recording plane using two flat mirrors. The mirrors are installed on computer-controlled rotary stages, allowing the angle of interference to be precisely controlled, and consequently the period of interference with accuracy better than 0.2 nm. The photosensitivity of PTR allows this interference pattern to generate a latent image inside the volume of the glass that can then be developed with thermal treatment (Fig. 7).

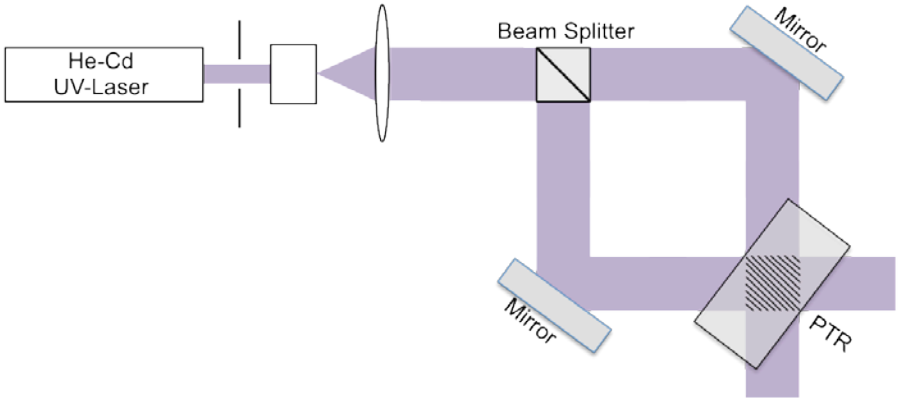

Figure 7: Setup for recording volume Bragg gratings in PTR via interference of two expanded collimated UV-beams at 325 nm.

To record a chirped Bragg grating in PTR glass, two cylindrical lenses are added in the path of each of the two split beams prior to their interference. These cylindrical lenses act to converge one beam and to diverge the other. The interference pattern generated from a convergent and divergent beam allows for a linear increase in the spatial frequency across the aperture. This feature enables recording a Bragg mirror with a linear variation of the spatial frequency along the beam propagation. By controlling the convergence and divergence of the recording beams, this increment in spatial frequency, or chirp in the interference pattern can be adjusted.

1.4 Important Parameters of Chirped Bragg Gratings

There are several important parameters that define a chirped Bragg grating in PTR glass. The first is the thickness of the CBG, as it defines the maximum allowable stretching time. Let us consider a pulse with a spectrum that overlaps with the reflection spectrum of the CBG. For a

pulse propagating along the z-axis, the shortest wavelength component is reflected from the front of the CBG, where the grating period is shortest, while the longest wavelength component is reflected from the back of the CBG, where the grating period is longest (Fig. 8).

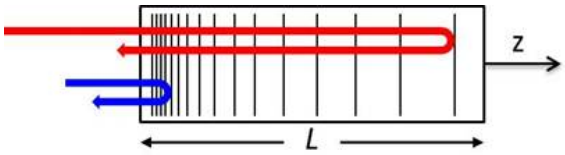

Figure 8: Spectral dependent time delay on chirped Bragg grating with thickness *L*.

Thus a wavelength dependent time delay between the different spectral components of the pulse is established, due to the different path lengths travelled by each spectral component. The stretching time (t_{stetch}) can then be calculated as below, Eq. (1.1).

$$t_{stretch} = \frac{2Ln_{avg}}{c} \qquad (1.1)$$

Where L is the distance between grating areas resonant for blue and red spectral components of the laser pulse, n_{avg} is average refractive index of a CBG, and c is speed of light. For PTR glass, with $n_{avg} = 1.5$, this stretching time is t_{st}(ps)=100L(cm). Thus, it is seen that very thick CBGs are required in order to achieve long stretching times.

Several other important parameters governing a CBG are derived from its spectral response (Fig. 9).

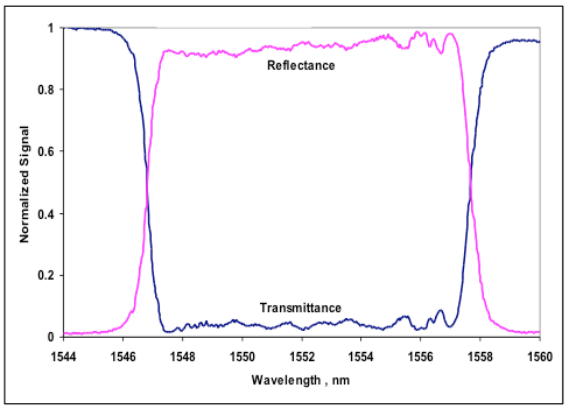

Figure 9: Spectra of diffraction efficiency (pink) and transmission (blue) of a 3cm thick CBG centered at 1552 nm with a bandwidth of 10 nm.

From this curve, the first critical parameter is the central wavelength of the CBG, which is determined by the average angle between the two recording beams used during fabrication and the average refractive index of the glass. Typically, CBGs can be manufactured with central wavelengths ranging between 700 and 2500 nm. A second critical parameter is the bandwidth of the CBG, and this is determined by the convergence and divergence of the recording beams. Typical bandwidth ranges are from a few nanometers to a few tens of nanometers. A final parameter is the level of spectral losses, mainly scattering losses inside the CBG. Each spectral component of an incident pulse travels a different propagation length inside the CBG, and thus the scattering losses are spectrally dependent. Typically, losses at the central wavelength vary between a few percent to a few tens of percent depending on the Bragg wavelength and the CBG parameters.

One of the most critical parameters defining a CBG is its group velocity dispersion (GVD), a parameter that depends on the spectral bandwidth of the VBG, its thickness and the linearity of the chirp. This parameter can be measured using for example a low coherence

interferometric system [1.26]. A typical GVD measured in a CBG recorded in PTR glass is shown in (Fig. 10). It is clear that this GVD is mostly linear but possesses some very small non-linear oscillations. This non-linearity is critical, as it represents higher order dispersion that cannot be easily compensated in CPA systems and therefore results in an increase of the pulse duration after stretching and compression. This is therefore one of the most critical parameter for the design and fabrication of CBGs in PTR glass.

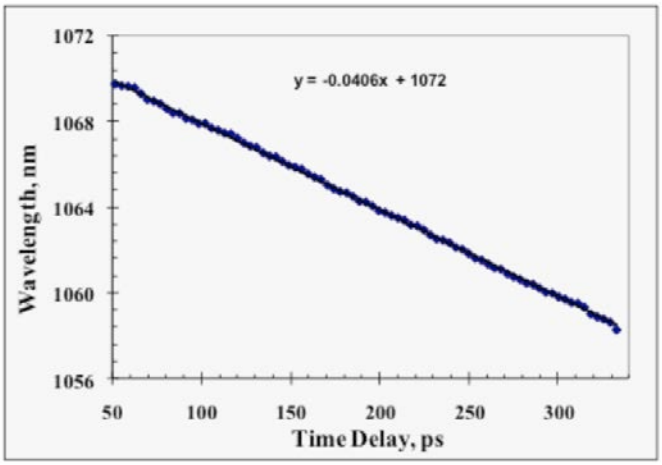

Figure 10: Group velocity dispersion of 3 mm thick CBG at 1064 nm.

The last important parameter defining a CBG is the quality of the beam following diffraction on said CBG. This is the parameter of interest that has been thoroughly investigated in this thesis. It is a critical parameter, as ultra-short pulse lasers are generally used to achieve high peak powers at the focus of the beam, and because the beam quality is directly responsible for the smallest spot size that can be achieved.

1.5 Stretching and Compressing with CBGs

The principle operation of a linearly chirped volumetric Bragg grating stretcher/compressor is that the different spectral components of an incident laser pulse are reflected at different refractive index planes within the grating and thus experience different time delays. The essential difference between volume Bragg gratings and fiber Bragg gratings is that a fiber grating aperture is limited by the size of the core, approximately 10 μm diameter, while the aperture of a volume Bragg grating is in principle unlimited. Therefore, increasing the size of the beam allows the energy of a pulse to be scaled up without damaging the device.

Moreover, volume Bragg gratings can be made with thicknesses suitable for 1000 ps or more stretched pulse duration. The duration of the stretched pulse dictates the amount of energy that can be added to the pulse through optical amplification. CBGs for 1 μm spectral range can be recorded with spectral widths from 20 to 30nm, thus enabling lasers capable of producing 200-1000 fs pulses.

A typical geometry of a CBG based CPA system is shown in (Fig. 11). This system is seeded with a femtosecond laser pulse that is directed into the CBG. The diffracted pulse exiting the CBG is then coupled into a fiber amplifier. The output from this first stage of amplification is down converted to 50-kHz using an acousto-optic modulator (AOM) and then launched into the second stage amplifier for further amplification. The pulses are then launched into the same CBG from the other end with a lateral offset from the stretching beam. Such a system was demonstrated at 1557nm for low power laser system [1.27], and at 1050 nm for high power [1.28]. Successful demonstration of such system paves the way for further development of CBGs in PTR glass.

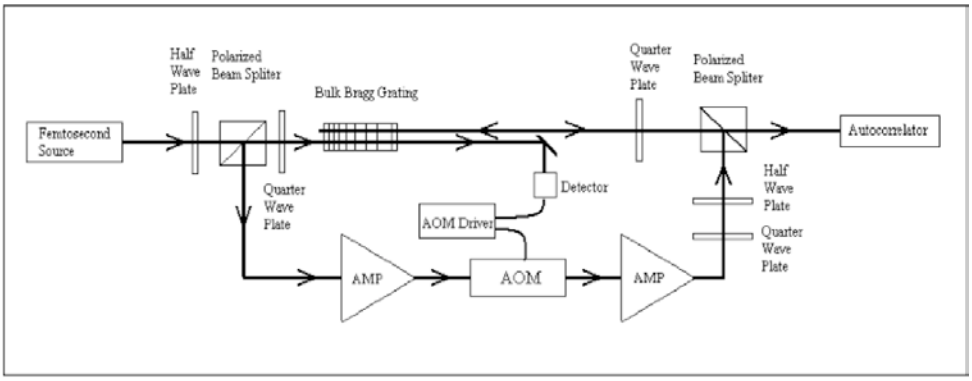

Figure 11: Schematic for a volume CBG based CPA system.

The ability to use the same grating for both pulse stretching and compression is key advantage of chirped Bragg gratings. Although the size of a proposed element will be relatively small, a 5×12 mm^2 aperture, the lateral size is large enough to allow two beams propagate parallel to each other within the grating. This makes it possible to stretch and compress a pulse using the same grating. Therefore, frequency chirps generated by the grating during stretching and compressing, would cancel each other, thus, minimizing the chirping distortion. This is a significant advantage over the hollow-core photonic bandgap fiber stretchers/compressors, in addition to CBGs orders-of magnitude higher energy handling capability.

CHAPTER TWO: MEASURING THE QUALITY OF BEAMS DIFFRACTED BY CHIRPED BRAGG GRATINGS

There are many attributes concerning laser performance, though none more common than the measure of beam quality produced by a laser system. Proper measurement of the profile and evolution of the beam as it propagates is highly sought after by many in the laser community. However, for one of the most demanded attributes concerning laser performance, beam quality is one of the least understood in terms of a proper way to measure it, as well as quantify it, mainly because the proper definition of beam quality depends strongly on the lasers specific application. However, even with the ambiguity present in the definition of beam quality, M^2 is still emerging as the primary measure of quality amongst those in the laser industry [2.1].

2.1 Review of Beam Quality Measurements

Any single-value measure of beam quality essentially encompasses two parameters of the beam, how tightly it can be focused and its far-field divergence. Gaussian beams represent a type of physical beam that can be focused to the tightest spot size with the lowest divergence. However, any distortions present in the optical wavefront of the beam limit its ability to be focused. Thus to measure the quality of a laser beam, the question becomes immediately, how is the width of the beam defined?

There have been numerous proposed methods for estimating the diameter of a beam (beam width), each with its own advantages and disadvantages. One of the simplest and earliest techniques for measuring beam width and one that is still used today for a quick estimate of the beam diameter is the knife-edge method [2.2]. In this method, the edge of a blade is translated

across the beam, effectively blocking a larger and larger area of the cross section. Using a power meter to record the power remaining in the unblocked portion of the beam, and plotting this power versus the position of the blade, a curve of the integrated power of the beam is obtained. The diameter of the beam is then defined with respect to this curve as the distance between two points that lie at a specified fraction of the total power, typically 10/90 or 20/80, as shown in (Fig. 12).

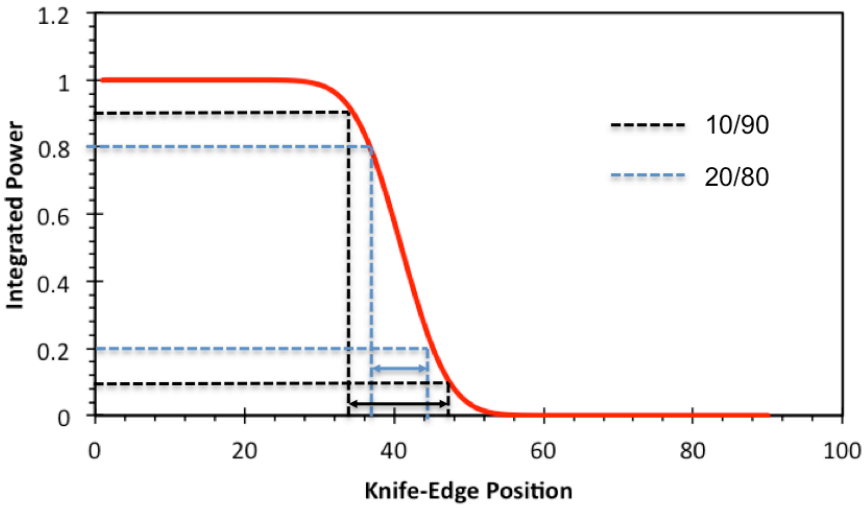

Figure 12: Theoretical plot of the integrated power of a beam measured via the knife-edge method. Beam diameter is defined as the distance between two points that lie at a given power fraction, typically 10/90 or 20/80.

Today modern techniques for measuring the diameter of a beam are based on measurements of the cross sectional profile of the beam. The transverse profile can be measured using a power detector and a small enough slit to sample the beam or a CCD camera that simply takes a snap shot of the intensity distribution. Using either method, the simplest way to define the

diameter of a beam from its transverse profile is its full width half maximum (FWHM). In this definition, the beam width is defined as the distance between two diametrically opposite points at which the intensity is half of the peak intensity. For most laser systems however, the output beam profile is Gaussian, and it becomes advantageous to define the beam width according to the $1/e^2$ standard [2.3]. In this case the diameter of the beam is defined as the distance between to diametrically opposite points at which the intensity is $1/e^2 = 0.135$ of the peak intensity of the beam. While these two definitions of beam width offer simplicity in calculation, they fail to represent the full characteristic of the beam. Two beams may share the same beam width yet have completely different beam profiles as shown below in (Fig. 13).

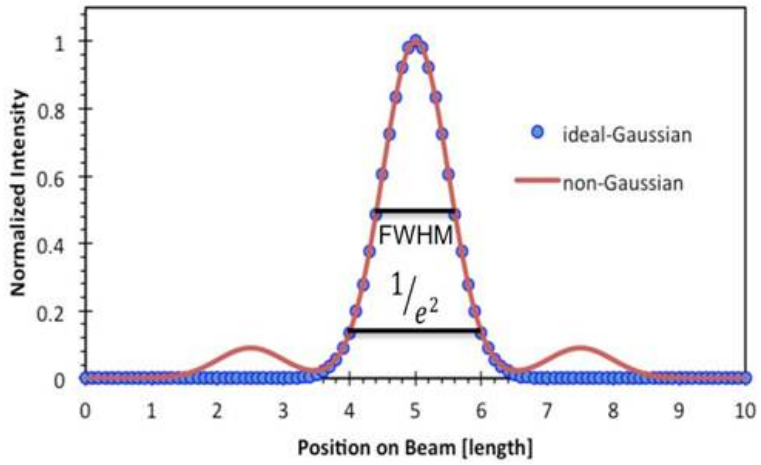

Figure 13: A Gaussian and non-Gaussian beam may have the same beam diameter as measured by the FWHM and $1/e^2$ definitions yet have very different beam profiles.

For a more complete definition of beam diameter, one that includes the influence of irregularities in the beam, the D4σ (second moment) width can be used [2.4]. In this definition,

the diameter of the beam is defined as four times the standard deviation of the beam intensity distribution, shown below in Eq. (2.1 – 2.2).

$$D_{4\sigma} = 4\sigma = 4\sqrt{\frac{\int\int I(x,y)(x-\bar{x})^2 dxdy}{\int\int I(x,y)dxdy}} \quad (2.1)$$

$$\bar{x} = \frac{\int\int I(x,y)xdxdy}{\int\int I(x,y)dxdy} \quad (2.2)$$

Where $I(x,y)$, is the beam intensity distribution along the x and y direction and $\bar{x}$ is the center of mass of the beam (COM). This statistical definition of beam width is sensitive to any distortions in the profile of the beam and thus allows for a full characterization of the beam. However, because of the squared term in the equation $(x-\bar{x})^2$, this definition is especially sensitive to distortions far removed from the central lobe of the beam. The calculated diameter is highly influenced by not only background noise, but by the sensitivity of the detector itself. Even still, the second order moment is still the most commonly used definition of beam diameter, in part because it is consistent with the $1/e^2$ definition for Gaussian beams and because it allows one to define the width of non-Gaussian beams as well.

With the various definitions of beam width now set in place, in order to establish a quantity that represents the quality of a laser beam a second parameter of the beam is required: its far field divergence. The far field divergence of a laser is essentially a measure of how fast the beam expands in the far field. This far field is associated with points beyond the Rayleigh length of the beam, which corresponds to points beyond where the beam radius has grown to $\sqrt{2}w_0$, i.e.

where the cross sectional area has doubled. This far field divergence can be quantified as an angular measure as shown in (Fig. 14).

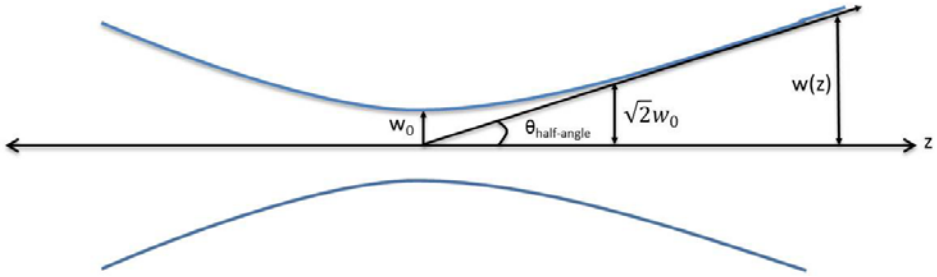

Figure 14: Definition of far field divergence.

This half-angle far field divergence is calculated as the derivative of the beam width with respect to the propagation distance in the far field [2.7], Eq. (2.3).

$$\theta_{half-angle} = \lim_{z\to\infty} \frac{w(z)}{z} \qquad (2.3)$$

With these two parameters, spot size, and far field divergence, a single value metric representing the quality of the beam can now be defined. Two common methods used today are the beam parameter product (BPP) [2.5] and the M^2 metric [2.5, 2.6].

The beam parameter product is simply the product of the beam radius at the beam waist (w_0), and its half angle far field divergence ($\theta_{half-angle}$), Eq. (2.4). It is a valuable metric that indicates how tightly a beam can be focused, and how quickly it will diverge from this focus.

$$BPP = w_0 \cdot \theta_{half-angle} \qquad (2.4)$$

A key feature of the BPP is its invariance under linear transformations, thus the BPP remains unchanged after focusing through a thin lens. This is useful, because focusing the beam with a lens brings the beam waist to the focal spot of the lens, providing a convenient method to measure the radius of the beam at its waist, as well as the half-angle far field divergence of the beam, (Fig. 15).

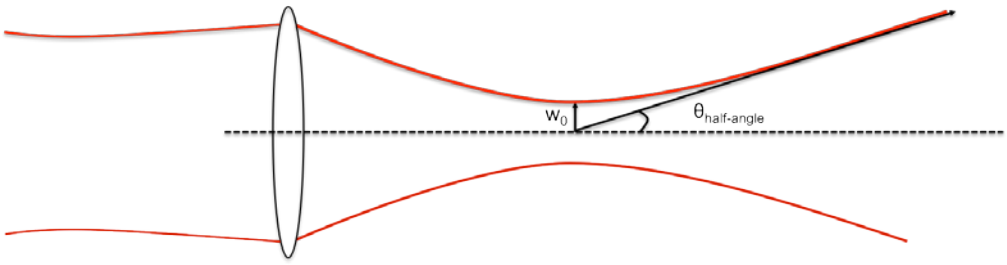

Figure 15: Focusing a beam with a lens brings the beam waist to the focus and allows for a convenient way to measure not only the radius of the beam at the waist, but also its far field divergence angle.

The second metric of beam quality mentioned, and the most widely used, the M^2 factor [2.5, 2.6] is defined as the ratio of the beam parameter product of a real beam (BPP_{beam}), to that of a diffraction-limited Gaussian beam at the same wavelength (BPP_0), as shown in Eq. (2.5).

$$M^2 = \frac{BPP_{beam}}{BPP_0} \qquad (2.5)$$

The M^2 metric uses the second order moment to define the radius of the beam, and is essentially a measure of how closely a beam resembles a Gaussian beam. From the definition of

M^2, it is clear that if a beam is Gaussian it will have an $M^2 = 1$. However, a non-Gaussian beam will have a larger BPP and thus an $M^2 > 1$.

The M^2 factor is an extremely useful metric, that not only represents how closely a beam resembles a diffraction-limited Gaussian beam, but it indicates how tightly it can be focused, as well as how quickly it will diverge. However, because the M^2 metric is based on the second order moment definition of beam width, it is sensitive to any distortions in the beam, especially those far removed from the central lobe. Thus, a large M^2 resulting from small wings far in the tail of the intensity distribution implies poor beam quality, even if the majority of the beam power propagates nearly diffraction-limited, (Figure 13). For many applications these small disturbances in the tails of the profile make no difference and so the deterioration in quality as measured by M^2 is quite often overestimated for these applications.

One way of compensating for this overestimation of beam quality deterioration is measuring the power in the bucket (PIB) curve [2.7]. The PIB is a measure of the fractional power contained within a predefined width, or bucket as it is called, measuring this fractional power versus the size of the aperture generates the PIB curve, (Fig. 16).

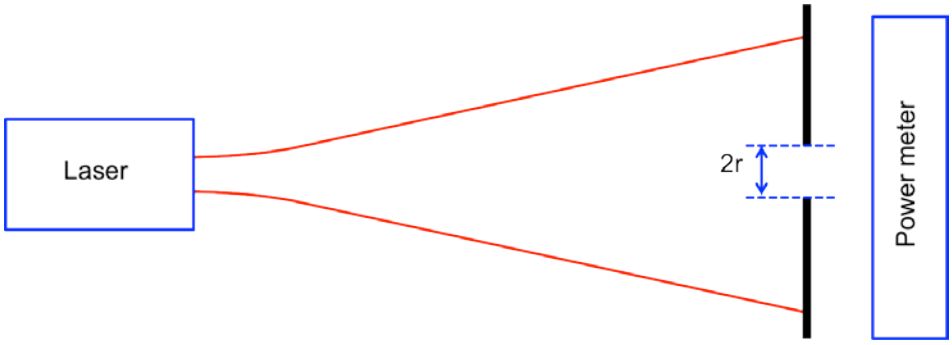

Figure 16: PIB is a measure of the fractional power contained with a predefined aperture. Measuring the fractional power as a function of the aperture size produces the PIB curve.

Measuring the power in the bucket offers a lot of insight regarding the quality of the beam. It says exactly how much power is contained within the central lobe at a certain location (most generally in far field), and it indicates how much power can actually be delivered to a remote location. For many applications, a thorough understanding of the power contained with a given area of the beam, as well as how effectively that power can be transferred over a distance and delivered to a remote target is sometimes all that matters.

For that purpose, we propose a new definition of beam quality coined S^2, that offers an insightful perspective on the quality of beams and helps resolve some of the inaccuracies of the M^2 method. The beam diameter for this new S^2 metric is defined from the transverse beam profile as the smallest diameter containing a certain pre-defined fraction of the total power. By measuring the beam radius according to this definition at different positions along the beam propagation, it becomes possible to define a new beam width at the focal spot as well as a new beam divergence. Thus, a new BPP can be calculated from this new definition of beam diameter, and by calculating the ratio between the BPP of the actual beam to that of the BPP of a perfect Gaussian beam using this new power fraction definition of beam diameter, the S^2 factor can be obtained.

2.2 Custom Beam Profiler

In this thesis we present the challenges associated with measuring the quality of beams diffracted by chirped Bragg gratings, as well as the inaccuracies associated with the standard M^2 metric. We show that the true M^2 value of a beam is not always easily obtained using a

commercial measurement system, and so we present a comparison between the M^2 method and our newly defined S^2 method and demonstrate the robustness of this new S^2 metric.

In order to perform such a complex analysis of various measurement methods, a common setup for measuring the transverse profile of the laser beam is needed. Thus, a custom beam profiler shown in (Fig. 17) has been developed, that enables accurate and sensitive measurements of the transverse profile of a laser beam diffracted by a CBG.

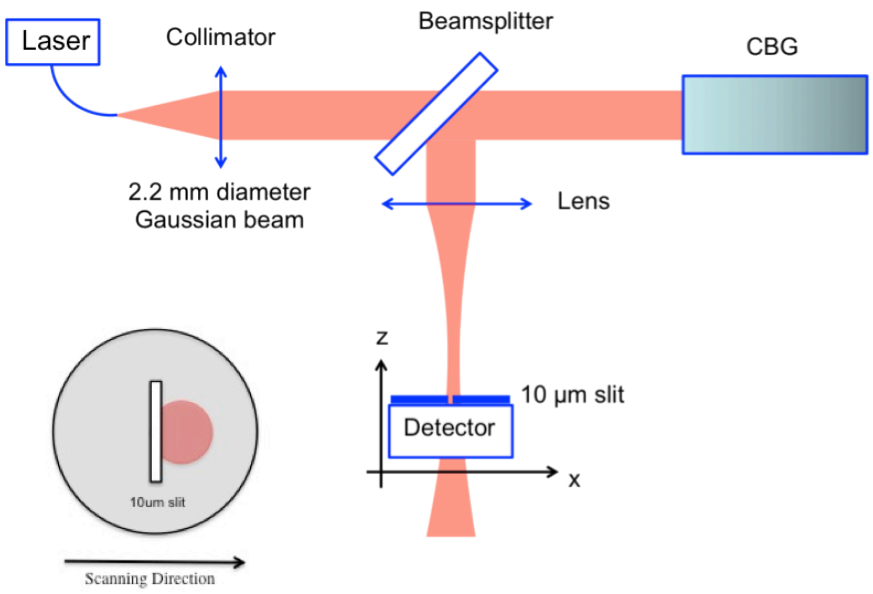

Figure 17: Custom beam profiler developed for accurately recording the transverse profile of beams diffracted by chirped Bragg gratings.

The light source is a femtosecond laser centered at 1550 nm. The beam is collimated using a commercial pigtailed collimator in order to produce a Gaussian beam with a 2.2 mm diameter (at $1/e^2$) and an M^2 close to 1. The beam is directed towards the CBG to be measured, and following diffraction on said CBG, a 50:50 beam splitter directs the diffracted laser beam

towards a focusing lens. A detector is mounted on translation stages that allow for movement across the transverse directions (x and y-direction) in order to record the profile of the beam, as well as along the beam propagation direction (z-direction) in order to map the beam profile at different distances from the focal plane of the lens. A 10 μm slit mounted to the face of the detector is used to sample the beam profile.

It is important to note that after such a slit the beam will be diffracted. Therefore, a complex pattern will be generated at the surface of the detector. Due to mechanical limitations, the slit could not be placed closer than 10 mm from the detector itself, therefore, it is not obvious whether all diffracted signals is captured by the detector or not, and whether this can have an impact on the measured signal. This point is very critical because it is seen that depending on the beam structure and how far from the waist the measurement is performed, the spatial and angular distribution of the beam intensity can vary and therefore the detected power and measured profiles can be different. In order to test this issue, three measurements were performed at the same z-position, but for each measurement the slits relative position in regards to the detector was changed shown in (Fig. 18).

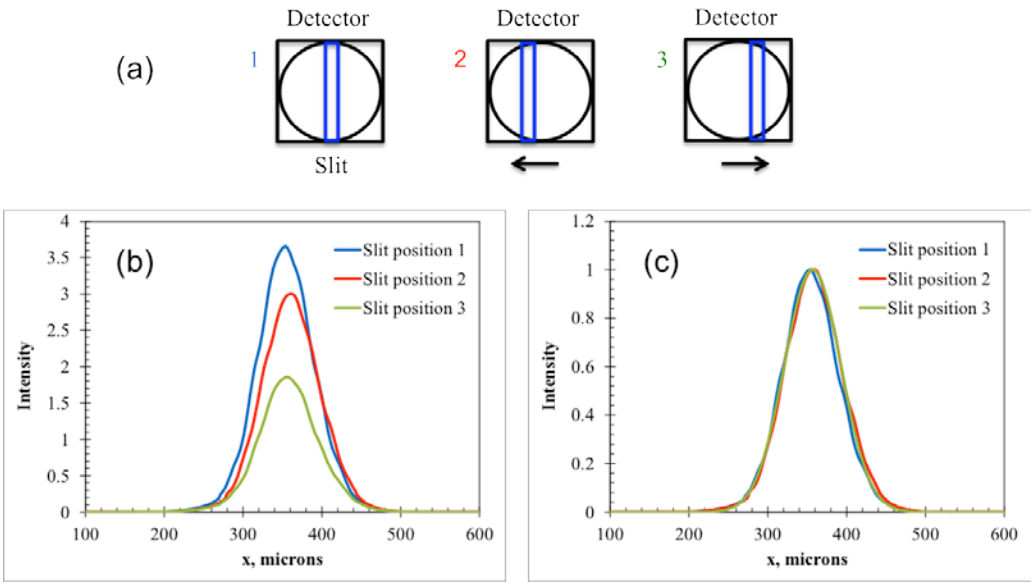

Figure 18: (a) Slit position translated with respect to detector. (b) Measured profiles at same z-position for each slit position show different measured energies for each profile. (c) Normalizing all three signals we see that measured profiles are the same.

It is clear that these three signals have significantly different intensity levels, confirming that diffraction by the slit has a significant impact on the measured signal. The signals were thus normalized in order to compare their profiles. What is clear is that although the detector captures different total energies, the relative fluctuations of the intensity over the x-direction are identical for all three measurements. Similar tests were performed on different beams at different z-position, all giving the same results. The conclusion is that diffraction of the beam by the slit and partial collection of the diffracted signal by the detector has no influence on the measured beam profiles.

The beam profiles measured along the propagation direction are then processed using custom Labview^{TM} coded computer programs. It is important that proper measurement acquisition and data processing allow obtaining low noise signals. Multiple tests have been

performed in order to be able to accurately separate the background (parasitic) signal from the useful signal of the measured beam. Using this setup it is therefore possible to accurately measure signals with a signal level below 0.1% of the maximum measured signal, anywhere along the z-direction. In other words, this system allows confidently detecting wings with amplitude 1/1000 or below the maximum signal, which is a critical parameter for the purpose of this work (Fig. 19a).

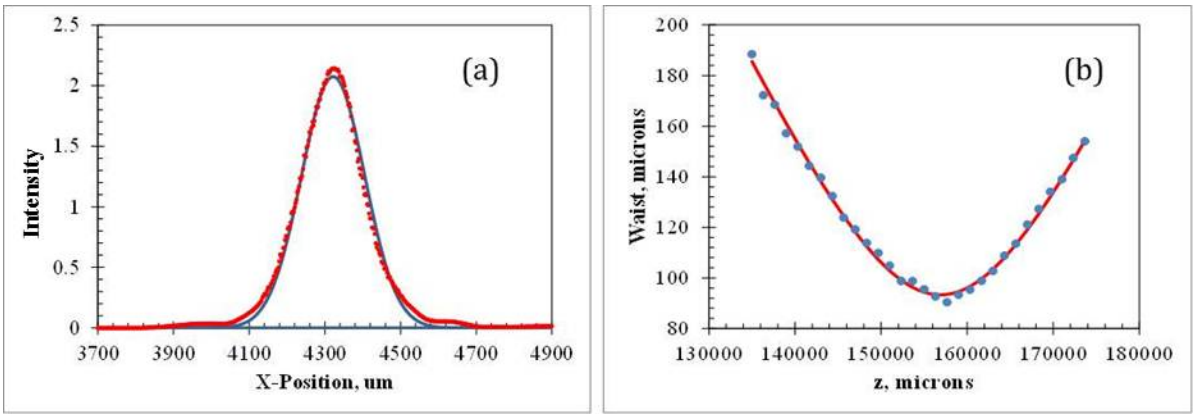

Figure 19: (a) Typical beam profile measured by custom developed beam profiler. System allows for accurate measurement of signal below 0.1% of maximum signal. (b) Typical caustic as measured by M^2 definition of beam width.

The beam radius is then calculated from each profile, the beam radius can be calculated according to both the M^2 and S^2 definition of beam width, and plotted against its z-position. Thus, two curves representing the evolution of the beam around the focus can be generated, one curve as measured by M^2, and one curve as measured by S^2. Since these curves have been generated from the same physical setup, they can now be compared, and thus a reliable test bed

for comparing both M^2 and S^2 has been developed. For illustrative purposes, (Fig.19b) shows a typical caustic of a beam diffracted by a CBG as measured by the M^2 definition of beam width.

2.3 M^2 Method

The M^2 method is the standard for measuring beam quality according to the International Organization of Standardization (ISO) [2.5] and is currently the most commonly used beam quality metric amongst those in the laser industry. The M^2 quality factor of a beam is defined as the ratio of the beam parameter product (BPP) of the beam to that of a diffraction-limited Gaussian beam at the same wavelength. One must remember that the BPP is a product of the beams radius at its waist and its far field divergence, and it can be measured from the beams caustic, a curve representing the evolution of the beam width away from its waist. Therefore, the M^2 factor of a beam can be calculated by measuring the evolution of the beam around its focus and calculating the factor that relates this caustic, to the evolution of a diffraction-limited Gaussian beam ($M^2 = 1$) at the same wavelength, (Fig. 20).

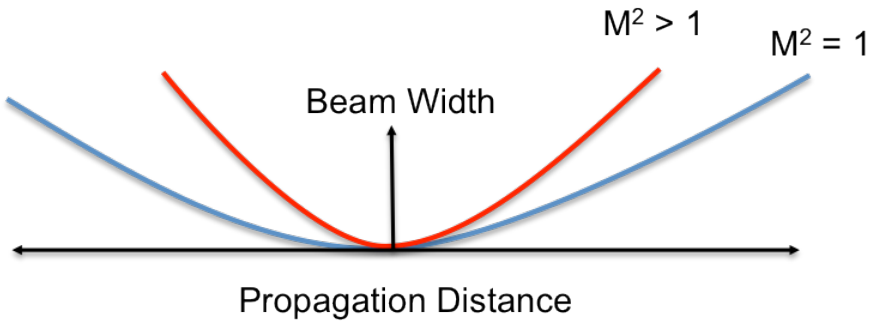

Figure 20: The M^2 metric is a factor that relates the evolution of the beam width away from the waist to that of a diffraction-limited Gaussian beam at the same wavelength.

The evolution a diffraction-limited Gaussian beam is given by the classical equation below [2.5], Eq. (2.6).

$$w(z) = w_0\sqrt{1 + \left(\frac{\lambda(z-z_0)}{\pi w_0^2}\right)^2} \qquad (2.6)$$

Where w_0 is the radius of the beam at its waist and z_0 is the position of the waist. Then for a non- Gaussian beam, one with an $M^2 > 1$, the evolution of the beam is given by Eq. (2.7).

$$w(z) = w_0\sqrt{1 + \left(M^2 \cdot \frac{\lambda(z-z_0)}{\pi w_0^2}\right)^2} \qquad (2.7)$$

When calculating the M^2 factor of a beam, the radius of the beam $w(z)$ is obtained from the recorded beam profiles by the second moment of the intensity distribution. However, because it is calculated from the second moment of the beam profile, it is highly sensitive to any distortions or noise in the beam profile. If the beam contains small wings in the tails of the profile, a low signal to noise ratio on the detector can have a significant impact on the resulting M^2 value. Therefore, measurements require proper handling of background noise, detector sensitivity, and baseline.

Even as sensitive a measure as M^2 is, many in the optics industry still rely on commercial profilers that commonly measure the M^2 of any beam. The problem with such systems is that the value of M^2 is obtained with no real understanding of the protocols that have been taken to give such value. To illustrate this we present the results of M^2 measurements performed on a CBG

using both our custom beam profiler and a commercial beam profiler. We show that subtle differences in the measurement procedure can lead to significant changes in the measured beam quality.

The commercial system is a Spiricon ModeScan Model 1780 [2.8] that measures the M^2 Beam Propagation Ratio and all associated ISO 11146 parameters [2.5] instantaneously in real time. The measurement technique is based on 10 reflective surfaces that form simultaneous images of the propagating focused beam at 10 locations on a CCD array camera. All ten measurements are acquired at once and beam diameters are obtained with NIST-traceable accuracy expected to be better than 2%. This translates to M^2 measurements with accuracy expected to be better than ~5%. As for the custom profiler developed in the lab, accuracy of beam diameter measurements was estimated to be within 2% and the accuracy of M^2 was determined to better than 5%.

Both systems were tested using a few mW, femtosecond laser oscillator at 1030 nm. In the commercial system, a focusing lens with a 200 mm focal length is used while the slit based system uses a 150 mm focal length lens. The two techniques using the same standards are thus expected to give very similar results. However, one main difference between the two measurements is that our custom system was designed such that the signal to noise ratio (SNR) at the detection system was decreased below 1/1000 at any position where the beam was measured. To ensure that only signal from the diffracted beam will be used in the second moment determination of the beam diameter in our custom system, a cutoff was set that defined background and noise as any signal corresponding to an SNR below 1/500. In other words any signal with amplitude smaller than the maximum amplitude dived by 500 was set to 0.

Experimental comparison between the two measurement systems first began with characterization of the quality of the beam reflected by a high quality flat mirror. Measurement with the commercial system gave an M^2_x along the horizontal direction of 1.09 and M^2_y along the vertical direction of 1.07. The results of the measurements using the custom based system were, an M^2_x along the horizontal direction of 1.14 and an M^2_y along the vertical direction of 1.06. The two values are very similar in the y-direction but present a small mismatch in the x-direction, however the difference is still within the error of the measurement technique for both systems (5%) and this difference in M^2 is too small to be debated here. The results are summarized below in [Table 1].

Table 1: Summary of M^2 results of beam reflected by plane mirror as measured by a commercial system and the custom beam profiler developed in the lab.

Plane mirror	**M^2_x**	**M^2_y**
Spiricon commercial profiler	1.09	1.07
Custom beam profiler	1.14	1.06

Following characterization of the initial beam quality using a plane mirror, a CBG centered at 1030 nm, with a thickness of 50 mm and a 7.5 nm bandwidth was aligned in place of the mirror and the quality of the diffracted beam measured. The results of the measurement using

the commercial system were an M^2_x of 1.18 and an M^2_y of 1.53. In comparison with results of the custom system which measured an M^2_x of 1.63 and an M^2_y of 1.55. The results are summarized in [Table 2].

Table 2: Summary of M^2 measurements after diffraction on CBG as measured by a commercial system and the custom beam profiler developed in the lab.

CBG	M^2_x	M^2_y
Spiricon commercial profiler	1.18	1.53
Custom beam profiler	1.63	1.55

Once more the two values are very similar in the y-direction but they present this time a large mismatch in the x-direction, well above the error of the measurement techniques. Therefore the beam profiles at each of the measured positions were analyzed, in order to understand this discrepancy between measurements. Unfortunately, the commercial system did not allow analyzing the exact beam profiles, but this could be performed using our custom slit based measurement system. In (Fig. 21), the beam profiles measured at the focal plane in both the horizontal and vertical direction, as well as the beam profiles measured after propagating 25mm away from this focal plane are shown. The red curve is the measured experimental data and the blue curve the best fitted Gaussian.

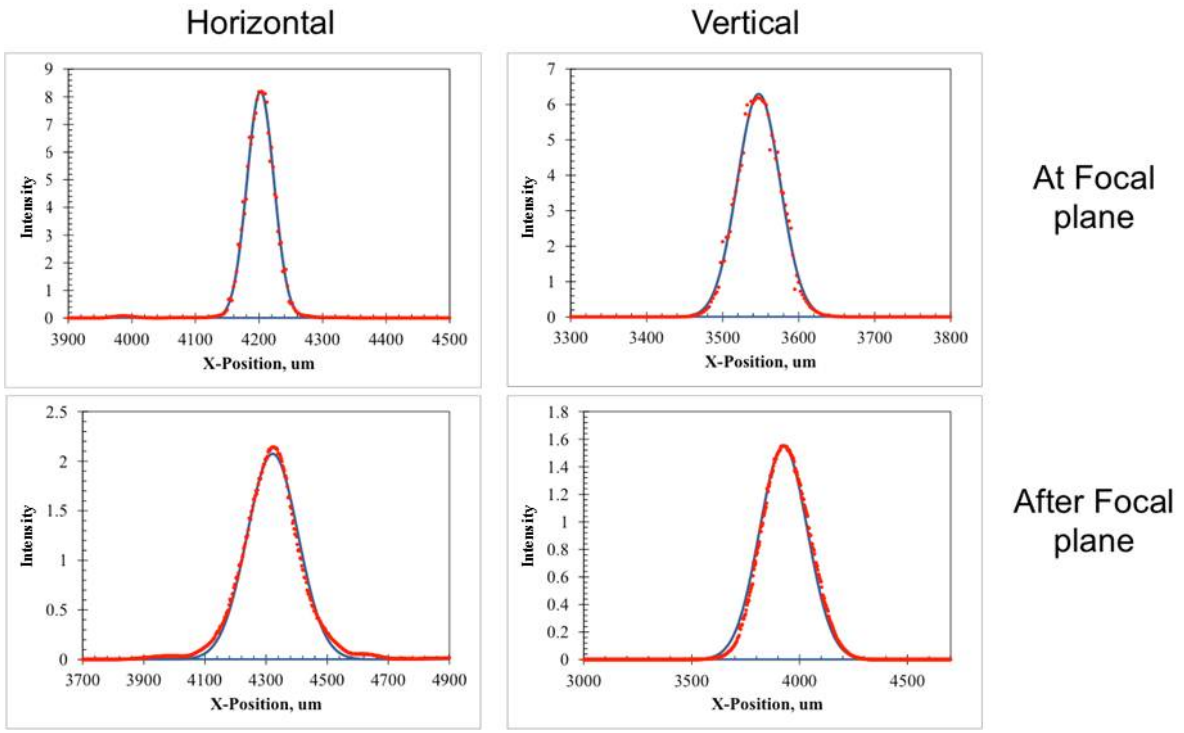

Figure 21: Horizontal and vertical beam profile measurements, recorded using our custom beam profiler, at the focal plane and outside the focal plane of a beam diffracted on a CBG.

It is clear that along the horizontal direction, the main lobe is narrower in comparison to the vertical direction, but contains the presences of some side lobes. As a result, because the M^2 metric defines the diameter of the beam according to the second moment of the beam, the main part of the central lobe centered at $\bar{x}$, has a minor contribution to the final beam diameter while side-lobes will have a significant impact due to the product of the measured intensity by $(x - \bar{x})^2$. Therefore it is clear that the increase of M^2 in the vertical direction is due to a broadening of the main lobe and is therefore easily detectable with any of the two measurement techniques.

However, the M^2-value measured along the horizontal direction is much more challenging. In our custom system, we defined a constant background corresponding to a SNR equal to 1/500, which is easily achievable at any place along the focused beam path, even if power density is decreasing as the distance measured from the focus increases. In regards to the commercial system however, it is based on a CCD camera coded with 12 bits, i.e. 4096 grey levels. Sensitivity of the camera is kept constant for all measurements and amplitude is automatically adjusted in order to fill the 4096 grey levels at the waist where the power density is the highest. Therefore, at the waist the lowest signal that can be detected is 1/4000 of the maximum signal, i.e. 0.025% of the maximum signal. While at the edges of the caustics, where beams have approximately 3 times larger waist, the lowest signal that can be detected is 1/400 of the maximum signal, i.e. 0.25% of the maximum signal in the center of the beam. If we suppose, in the best case scenario, that noise represent only fluctuations over 4 grey levels, background will be equal to roughly 1% of the maximum signal. In other word, the beam diameter cannot be properly determined using this commercial system if wings exist. To illustrate, the experimental data that was measured along the horizontal axis using the custom beam profiler was re-processed. For each beam profile the background level was varied from 0.2 to 2.5% of the signal with smallest intensity (achieved at the edge of the measured caustics), setting all data below this background to 0. The M^2-value was then recalculated as a function of the background, (Fig. 22).

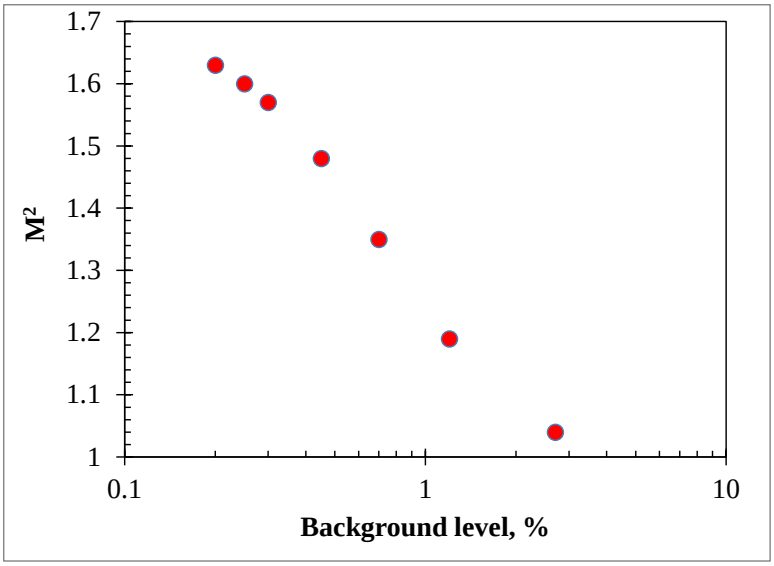

Figure 22: Effect of background level on the M^2-value extracted from a beam diffracted by a CBG and presenting side-lobes.

One can see that when wings are present in the beam profile, the background level highly influences the final M^2-value. Moreover, one can see that the estimation of a detection level of 1% of maximum signal with lowest intensity, gives an M^2-value equal to the one that was determined by this commercial setup ($M^2 = 1.18$).

What is gathered is that M^2 is a highly sensitive measurement, and the results from a commercial system cannot be seriously taken without proper understanding of the protocols taken to generate its value. Furthermore, even when proper protocol is taken in measuring M^2, the squared dependence in the second moment definition of beam width places such a large emphasis on signal far removed from the central lobe, that many times the deterioration in beam quality as determined by M^2 quite often does not give a representative metric of the final performances in a laser system [2.1, 2.9].

2.4 S^2 Method

In this thesis a new metric of beam quality is introduced that has been coined S^2. This new definition is introduced in order to help resolve some of the inaccuracies of M^2 for beams that have side lobes. This study applies broadly to all optical components affecting laser beams, but for experimental testing, the results of these two methods are compared on beams that have been diffracted by chirped Bragg gratings (CBGs).

The proposed S^2 metric, like the M^2 metric, is a ratio that relates the beam in question to that of a diffraction-limited Gaussian beam at the same wavelength. Where the two methods really differ is in their definitions of beam diameter. The S^2 metric, unlike M^2, calculates the diameter of a beam according to a power fraction method. The beam diameter is defined as the width of a symmetrical, rectangular slit, centered on the center of mass (COM) of the beam that encompasses a set fraction of the power. The power fraction that is used to determine the diameter of the beam can be set to any level. In our measurements we typically use power fractions corresponding to 95.6%, 90%, and 80% of the total beam power. Calculation of the diameter of a beam using this new method is shown in (Fig. 23).

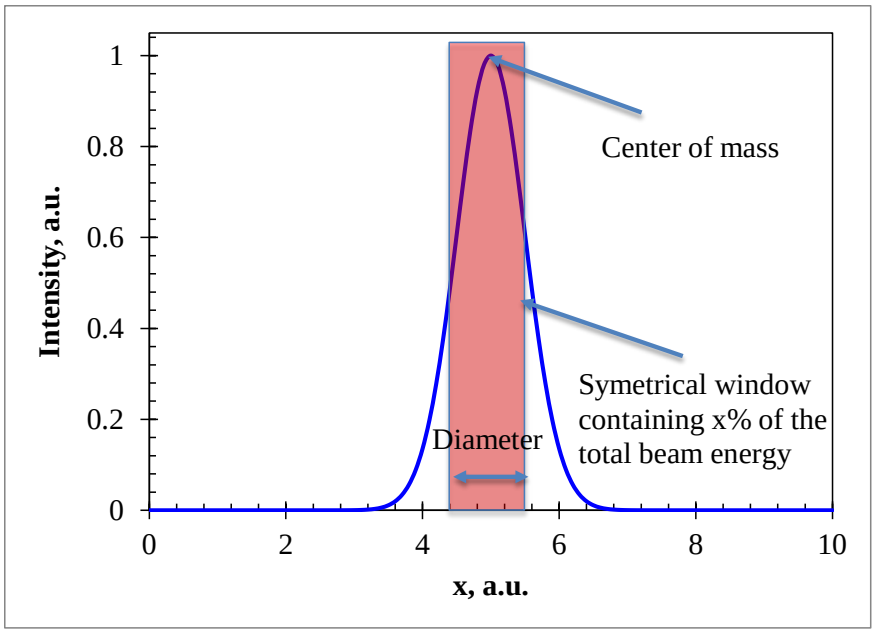

Figure 23: Definition of the power in the slit (PIS) extracted from each intensity profile measured along the beam propagation direction.

The center of mass of the beam (COM) is calculated from the same equation that describes the center of the beam ($\bar{x}$) in the second order moment equation, it is shown below in Eq. (2.8).

$$COM = \frac{\int\int I(x,y)xdxdy}{\int\int I(x,y)dxdy} \qquad (2.8)$$

The symmetrical rectangular slit, centered on the COM of the beam, is a theoretical aperture that only exists within the computer processing. The computer program continually increases the width of the slit around the center of mass, recording the power within the area of the slit, versus the width of the slit, essentially a measure of the power in the bucket versus the bucket size. (Fig. 24) below shows such a PIB curve, for a theoretical Gaussian beam profile.

The beam diameter for the 95.6%, 90%, and 80% power fractions can now be calculated from this curve, they are simply the bucket diameter at these power fractions.

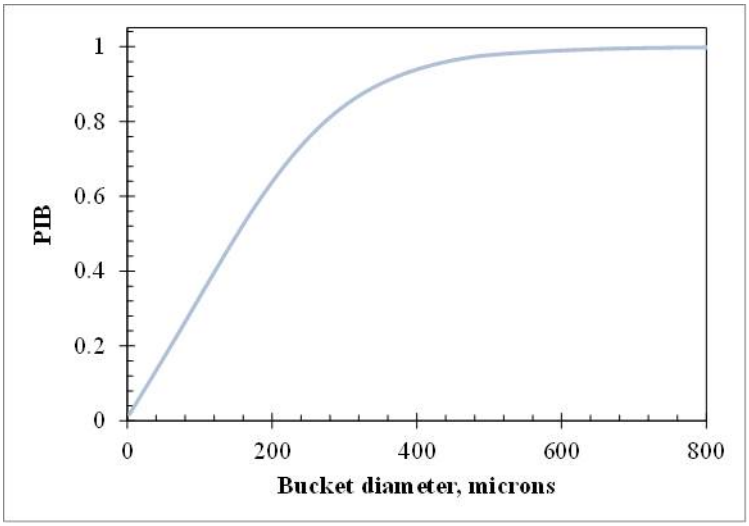

Figure 24: Normalized power in the bucket versus the width of a bucket for an ideal diffraction limited Gaussian beam profile.

Just as with the M^2 method, the radius of the beam is calculated at different distances from the focus according to the S^2 method. Using the beam radius calculated for each z-position, a caustic, just as in the M^2 method can be generated.

We started with a theoretical diffraction-limited Gaussian beam at 1.5 μm, with an $M^2 = 1$ within Labview™. The generated beam profiles were then processed according to S^2, using the three different power fractions (95.4%, 90%, and 80%) to calculate the beam radius. Three caustics according to S^2 method were thus generated, (Fig. 25).

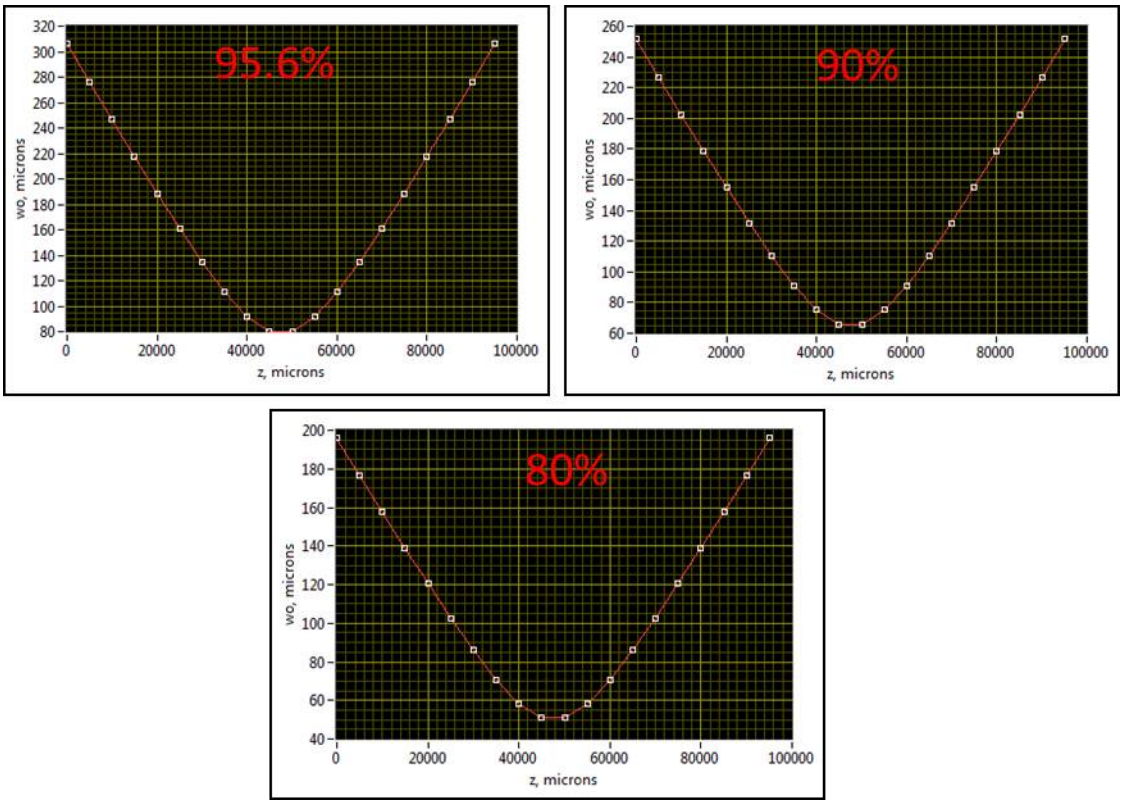

Figure 25: Caustics generated from S^2 measurements at 95.6%, 90%, and 80% power fractions on a computer generated ideal diffraction limited Gaussian beam ($M^2 = 1$).

These new generated caustics were then fitted with the following equation:

$$w(z) = w_0\left(1 + BQ^2\left(\frac{\lambda z}{\pi w_0^2}\right)^2\right) \qquad (2.9)$$

Where BQ^2 is a new beam quality factor as measured by the S^2 definition of beam width, and because only a fraction of the beam was used to determine its radius, the new corresponding BQ^2 values are ≤ 1.

For a perfect Gaussian beam at 1.5 μm with and $M^2 = 1$, we have:

- $BQ^2(95.6\%) = M^2 = 1$
- $BQ^2(90\%) = 0.67$
- $BQ^2(80\%) = 0.405$

Just as the M^2 factor is a ratio of the BPP of a real beam to the BPP of an ideal-Gaussian, the S^2 factor is the ratio of the BQ^2 factor measured for a real beam to the BQ^2 of a Gaussian beam at the same wavelength, and measured at the same power fraction.

$$S^2(x\%) = \frac{BQ^2(x\%, measured\ beam)}{BQ^2(x\%, Gaussian\ Beam)} \qquad (2.10)$$

Thus, to calculate S^2 for a non-Gaussian beam, the beam radius is calculated using one of the pre-defined power fractions above. The resulting caustic is then fitted and the corresponding BQ^2 is calculated. Dividing this BQ^2 factor by the corresponding BQ^2 factor for a diffraction-limited beam at the same wavelength and the same defined power fraction, the resulting S^2 value is obtained. In (Fig. 26), a typical measurement of S^2 using 90% and 80% power fraction definitions on a non-Gaussian beam diffracted by a CBG is shown.

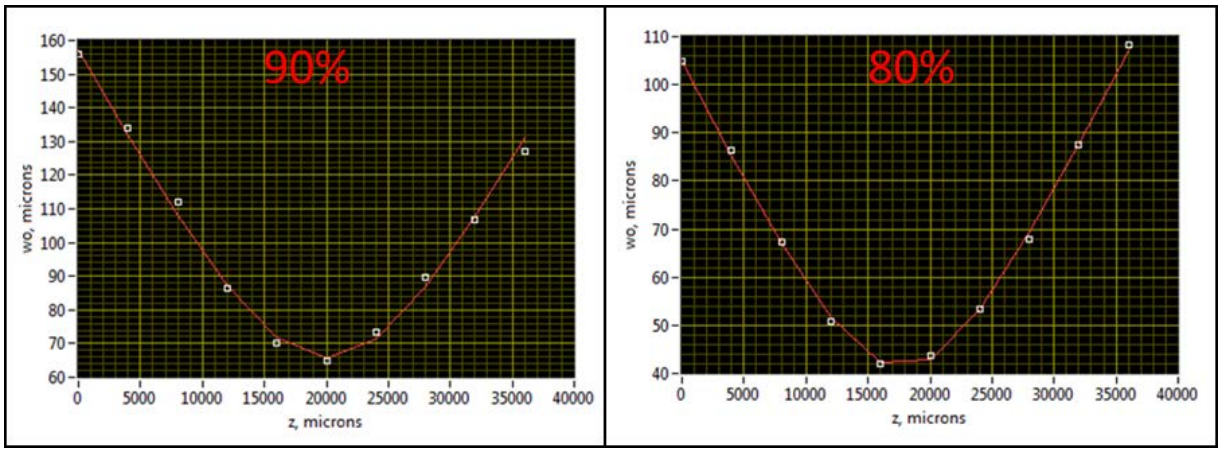

Figure 26: S^2 caustics generated from beam diffracted by CBG, with beam diameter measured by 90% and 80% power fractions.

One can see that similar caustics as the ones obtained for M^2 measurement are calculated. Moreover, all the equations used previously for fitting the evolution of the beam width around the focal plane can be used. One can see that the calculated curves are perfectly symmetrical. At this stage, it is important to note that all these curves, for both M^2 and S^2 measurements should be symmetrical. However, when measuring M^2, it is commonly observed that there is an asymmetry that the beam is diverging more, either before or after the focal plane. This asymmetry has no physical existence it is a result of the fact that beam diameter was not measured properly, i.e. that a fraction of the power was not detected and therefore not taken into account for the determination of the second moment, as is common with M^2 measurements. With the new S^2 definition, such large errors are prevented, and therefore, more accurate beam quality measurement can be achieved.

2.5 A Comparison of the M^2 and S^2 Method

To compare the two methods, M^2 and S^2 measurements were performed using the custom beam profiler on numerous CBGs. To present the results, we look at the particular measurements performed on a CBG presenting known specific beam distortions, [Table 3] below presents the M^2 and S^2 results for both the horizontal and vertical axis of the beam.

Table 3: M^2 and S^2 results measured on beam diffracted by a CBG.

CBG	**M^2_x = 1.5**	**M^2_y = 2.19**
S^2 (95.4%)	S^2_x = 1.4	S^2_y = 2.07
S^2 (90%)	S^2_x = 1.22	S^2_y = 2.06
S^2 (80%)	S^2_x = 1.13	S^2_y = 2.0

M^2 and S^2 results along y-axis are pretty consistent. However, along the x-axis measurements show some significant differences. Examining the horizontal beam profile at the focus of the lens used in the measurement setup clearly illustrates why there is such a large difference between the M^2 and S^2 methods (Fig. 27). The presence of a small wing ~200 μm away from the central lobe of the beam, and with amplitude only ~1% of the maximum signal level drastically influences the second order moment value and therefore increases the M^2 value.

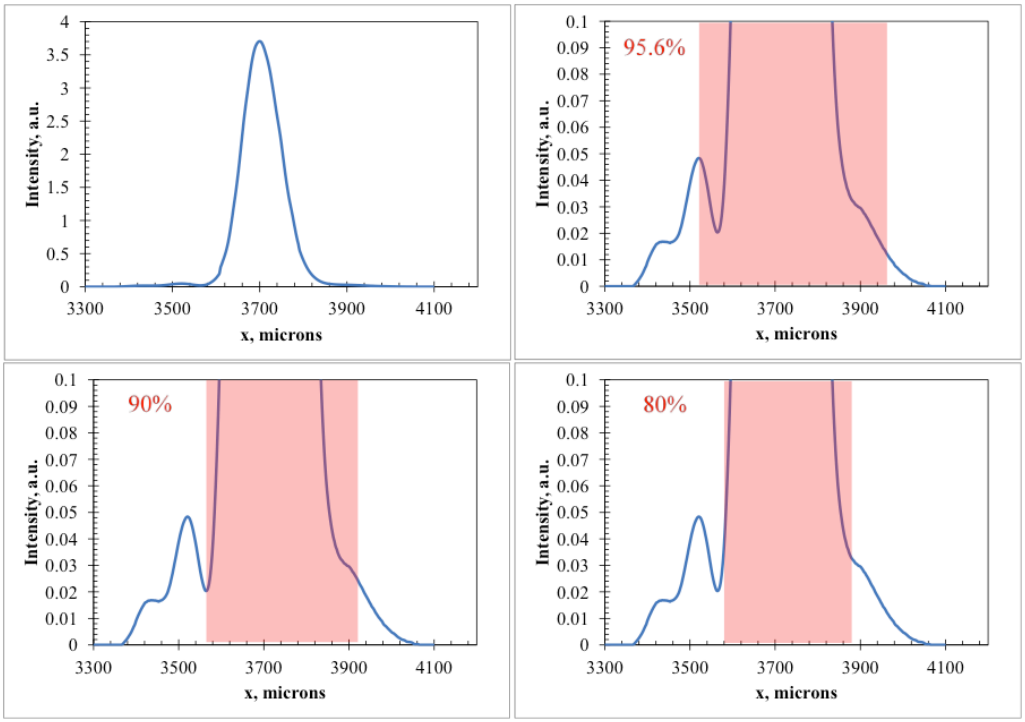

Figure 27: Beam profile at focus in x-direction and the windows used for extracting the beam diameters used for calculating S^2-value. The side-lobe results in an increase of the M^2-value while S^2-value has only a low sensitivity on this wing whatever the power fraction.

Actually this small wing places a large weight factor on signal far removed from the central axis due to the squared term within (Eq. 2.1). By allowing only a fraction of the power within the beam to define its overall quality, as in the S^2 method, the measured beam quality is improved. We see that as the power fraction decreases from 95.6% - 80%, there is less influence from the wing, as well as the broadening along the right side of the beam profile, and thus the measured beam diameter and likewise the S^2 value is smaller in comparison to M^2.

It is important to stress that the goal of this new definition is not to obtain better values of beam quality, but to allow differentiating different types of beam deteriorations, to decrease the influence of errors in the background/signal differentiation, and to describe the real power

that would be delivered to a remote target in a collimated or focused beams. As shown in the example, a beam in which deterioration is produced by a wider divergence of the central lobe containing most of the energy will present very close M^2 and S^2 values (See y-axis). However, a beam which is deteriorated by the appearance of small wings containing only a small fraction of the total energy will generate a large M^2 but a small S^2 (See x-axis).

In order to demonstrate the usefulness of the S^2 metric, and show that it is in good agreement with M^2 metric for most beams, but offers an insightful perspective for beams that have been deemed poor by the M^2 method. We present the results of a large number of S^2 and M^2 measurements performed on CBGs and plot their corresponding values on the same graph (Fig. 28).

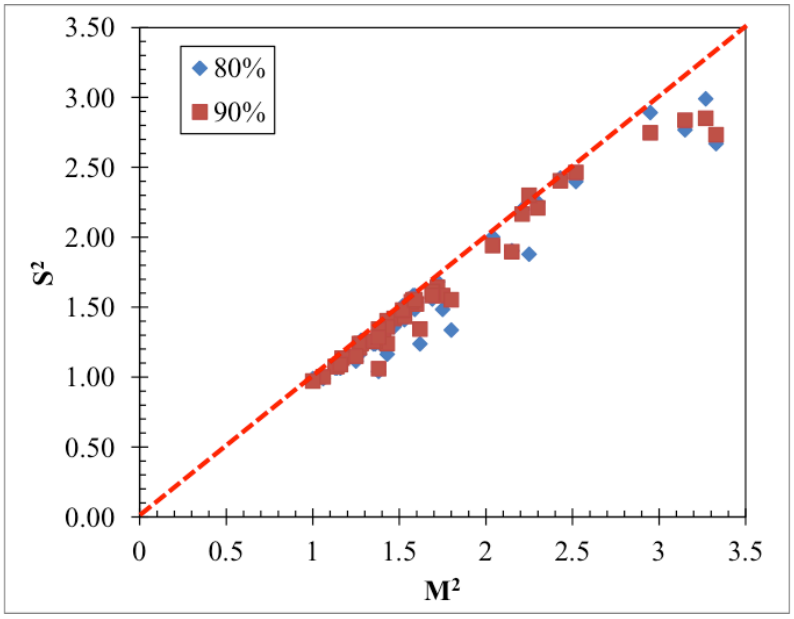

Figure 28: Statistical analysis of S^2 on M^2 measured on a large panel of CBGs (~40) with different properties, sources of distortions, and therefore beam profiles.

We see that for most beams, the M^2 and S^2 methods offer similar insight into the quality of the beam. However for beams with small disturbances in the tails of the profile, the M^2 metric quite often overestimates this influence resulting in a large M^2 value in comparison to a relatively diffraction-limited S^2 value (Fig. 29).

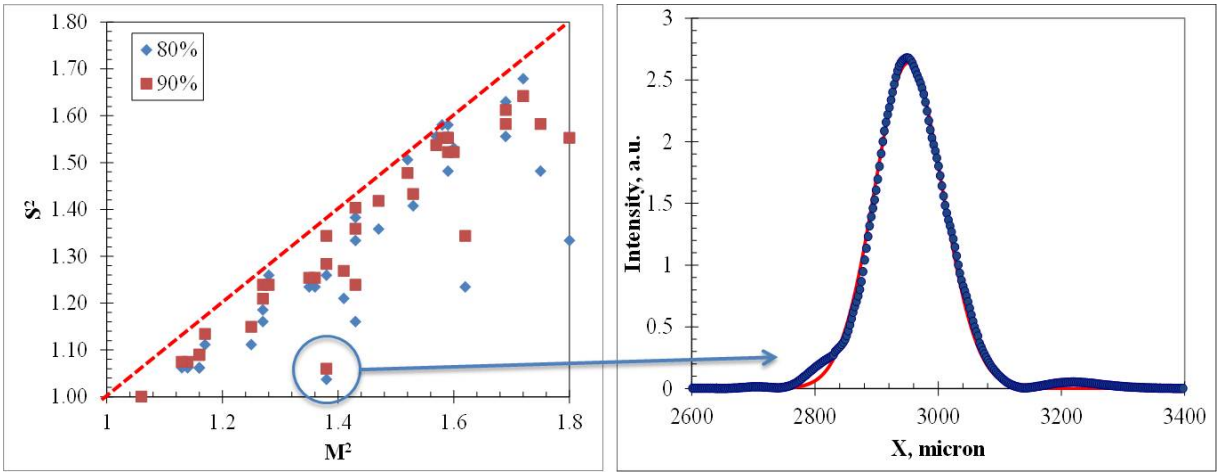

Figure 29: Beam Quality better understand with both M^2 and S^2.

Moreover, it is obvious that the contribution of this wing to beam quality will also depend on how the beam was measured and consequently on the signal to noise ratio. However, for most of the applications, the most important parameter is how much energy can be deposited on a given spot size and is therefore insensitive on the presence of small wings. In conclusion, the S^2 definition offers an insightful additional perspective to beams otherwise deemed "poor quality" by the accepted standard M^2 method, and so the performance of a beam having both parameters (M^2 and S^2) is predictable.

CHAPTER THREE: MECHANISMS OF BEAM QUALITY DETERIOARTION IN CHIRPED BRAGG GRATINGS

Chirped Bragg gratings recorded in photo-thermo-refractive glass offer many advantages both as a stretcher and compressor within femtosecond pulse CPA systems [3.1]. In particular, they offer the ability to stretch pulses on the order of 1 ns [3.2]. However, to achieve pulse stretching on this scale requires a CBG to be 10 cm long, and because some spectral components of a diffracted beam propagate through the entire length of the CBG twice, a stretched pulse will have propagated through up to 20 cm of PTR glass. Such large propagation distances through an optical material places strict requirements on the parameters known to deteriorate the quality of an incident beam.

In chapter 2, it was shown that one significant origin in the increase of the M^2-value of a beam is the presence of wings in the beam profile diffracted by CBGs. Moser et al. showed that one of the origins of this deformation of the beams is associated with a GRIN-effect due to the gradient of dosage produced during transverse recording of the CBG that results in the equivalent of fringes with linearly increasing tilt [3.3]. Other local distortions of the glass or recording beam can produce such mismatch of some local fringes and generate local wings due to the incoherent sum of all the diffracted wavelengths.

Actually, there are a large number of possible distortions of the beam quality (M^2). A non-exhaustive list is summarized below:

- Original glass optical homogeneity
- Thermally-induced heterogeneities
- Photo-induced optical heterogeneities (aberrations and fan)
- Gradient of refractive index
- Thermally-induced distortions (warpage)

Within this chapter we review the different possible sources of distortions in PTR glass.

3.1 Grating-related Distortions

As mentioned in the introduction, there are numerous sources of distortions in CBGs recorded in PTR glass. In this section we review the grating-related distortions. The first effect is associated with the recording process. As presented in chapter 1, the recording of CBGs is based on the interference of two wide aperture cylindrical beams, one diverging and the other one converging. One would expect that at the interference plane, the resulting fringes would be plane and parallel. However, it was shown that a fan of fringes occurs during the recording process when cylindrical convergent and divergent beams with slightly different radii of curvature form the interference pattern [3.4]. However, for the CBGs considered in this study, this effect has little impact on the resulting tilt (Θ_{max}) of the grating vector, which is defined as the angle

between the two fringes having the largest angle between their normal, as this tilt is expected to not exceed a few 0.01^{o}.

There are much more important effects that would result in a very significant decrease in the quality of the beams diffracted by CBGs. The first is associated with the recording process. CBGs are fabricated by holographic recording of plane parallel fringes with linearly increasing period in the z-direction, (Fig. 30). The recording beams propagate in the x-z plane and are collimated in this plane. The angle between the recording beams in x-z plane determines the average period of the grating. The angles of divergence and convergence of the recording beams determine the spatial chirp of the grating period. The photosensitive process is triggered by absorption of UV radiation by cerium ions. Therefore, it appears a gradient of absorbed dosage that will be converted into a gradient of refractive index (GRIN) along the x-direction of the CBGs.

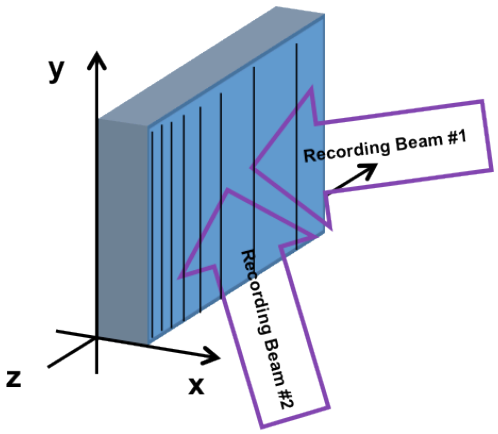

Figure 30: Holographic recording setup for CBGs. The angle between the recording beams in the xz-plane determines the average period of the grating. The spatial chirp is determined by the angle of divergence and convergence of the recording beams.

This GRIN then produces a mirage effect. Due to the different beam paths of each spectral component, each of them will be deflected to a different place, ultimately impacting the quality of the diffracted beam. More precisely, it was shown that a GRIN causes an incident beam as well as the diffracted beam to bend towards the gradient, resulting in the elongation of the beam in the vertical direction after diffraction on a CBG [3.4], (Fig. 31).

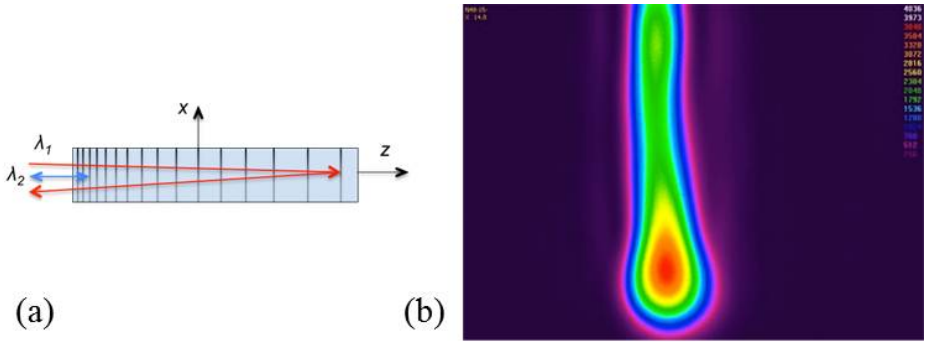

Figure 31: (a) CBG with GRIN along x-direction, resulting in vertical tilt of the grating vector. (b) Elongation of beam in vertical direction due to GRIN, as measured with a CCD camera.

GRIN results in a vertical tilt of the grating vector along the CBG's thickness that can be expressed in a term of a radius of curvature (R_{GRIN}) given by Eq. (3.1).

$$R_{GRIN} \approx \frac{1}{GRIN} \qquad (3.1)$$

Therefore, this effect is equivalent to a deformation of the overall glass following a close to spherical shape with the defined radius of curvature. It is important to note that this effect is a deterministic process that has been studied in detail and that can be theoretically predicted using

the absorption coefficient of the glass at the recording wavelength and the PTR glass refractive index change kinetics [3.5].

Another important grating effect is associated with the development process itself. To develop the photo-induced refractive index in PTR glass, it is necessary to thermally treat the glass at an elevated temperature above the glass transition temperature. At this temperature the glass is no longer solid and is closer to a liquid. While below the glass transition temperature, only elastic deformations occur, above the glass transition temperature, plastic deformations occur [3.6], resulting in irreversible deformations (warpage) when the glass is cooled down to room temperature (Fig. 32).

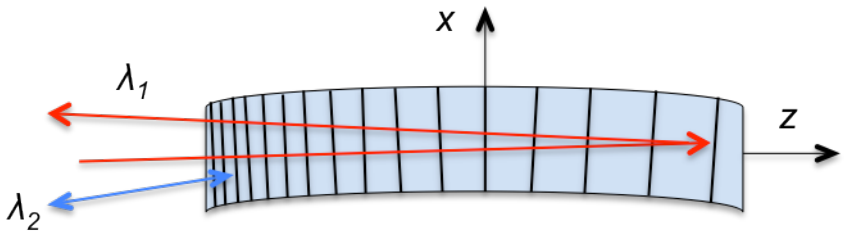

Figure 32: Physical warping of the glass occurs as it cooled to room temperature following thermal development.

It is important to note that this effect is not a parasitic effect specific to PTR glass, but a general effect that happens to all glasses, especially during thermal annealing. There are several effects at the origin of these distortions: uncompensated stresses on the glass surface, glass heterogeneities, gradient of temperature within the glass… that make this effect very difficult to control. Similar to GRIN, this deformation can be expressed into a radius of curvature according to the following formula, Eq. (3.2).

$$RoC = \frac{L^2}{8PV} \qquad (3.2)$$

Where L is the sample lateral size and PV is the peak-to-valley deformation along the z-direction, (Fig. 32).

It is interesting to get an insight on the amplitude of these deformations. Both GRIN and warpage tend to contribute with the same magnitude, the typical induced radius of curvature ranging from a few tens of meters to a few hundreds of meters. The angular divergence θ between the beam diffracted at the front of the CBG and the beam diffracted at the back of the CBG is given by Eq. (3.3).

$$\theta = 2\ Atan\left(\frac{L}{R_{GRIN}+R_{warp}}\right) \qquad (3.3)$$

The output beam is thus elongated along the vertical direction (Fig. 31), and because different spectral components are reflected at different refractive index planes within the grating, this elongation results in a spatial chirp. These deformations result in an M^2 after diffraction higher than 5 for the low radius of curvatures, to negligible increase of M^2 for the largest radius of curvature. A detailed theoretical analysis of the relationships between these distortions and the induced beam distortions was performed and can be found here [3.4]. In addition, large efforts have been made towards the developments of methods for the mitigation of these distortions, but they are beyond the scope of this thesis.

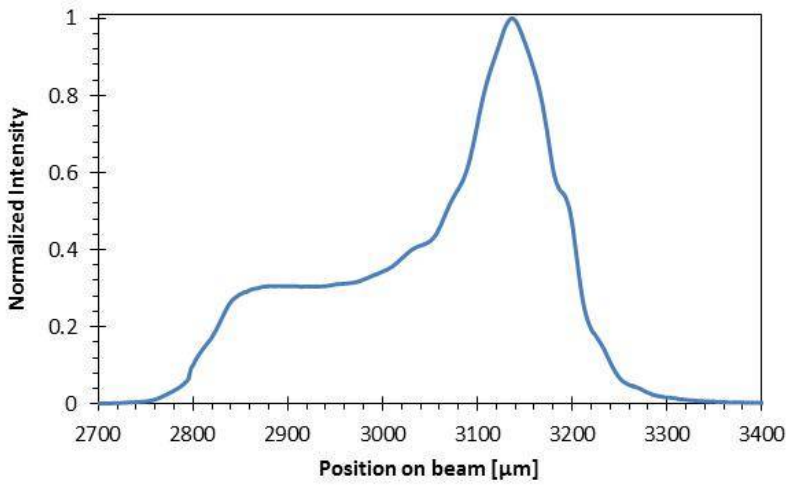

Figure 33: Beam profile measured after diffraction on CBG using our custom beam profiler. Elongation of the beam profile is due to GRIN and warpage, resulting in an $M^2 > 5$.

3.2 Glass-related Distortions

We have already reviewed several sources of beam distortions, all of them being associated with the grating itself. However, there is a more basic parameter of any optical glass that can distort a propagating beam, its optical homogeneity. Thus, the original homogeneity of the PTR glass used to record the CBG is critical. Random local variations of refractive index, or striae, throughout the glass matrix can deteriorate the quality of beams propagating through the glass. This is a very well-known and universal effect that the glass industry has been dealing with since optical quality glasses have been fabricated. As of today, each optical glass is provided with a certificate that indicates the maximum allowable fluctuations of the refractive index over its aperture [3.7]. This number, which is a key-parameter in the optical glass industry, is however hardly understood by the laser community, as it lacks direct correlation with the quality of a laser beam after propagation in such a glass. The only known fact is that the lower refractive index fluctuations over the aperture, the lower the beam distortions. We therefore

asked the question, how to relate the refractive index fluctuation over a glass aperture to the final beam quality after propagation? A theoretical investigation of how the quality of an incident Gaussian beam is affected by a glass that has been deformed by non-uniform heating has already been performed [3.8]. In this thesis, we have adapted this theory to the case of Gaussian beam propagation in a heterogeneous medium, and then have experimentally investigated this phenomenon.

There is no general solution to the task of modeling the effect of glass homogeneity on beam quality after propagation, because of an infinite number of possible profiles of striae in the glass or crystal, and an infinite number of possible orientations of these striae in respect to the direction of beam propagation. Therefore, we have developed a model that describes the propagation of a collimated beam through a medium with only lateral distortions of a refractive index. Let us consider the simplest case when a Gaussian beam propagates through a phase plate with a lateral (x-y) distribution of refractive index and uniform profile of refractive index in the direction of beam propagation z, (Fig. 34).

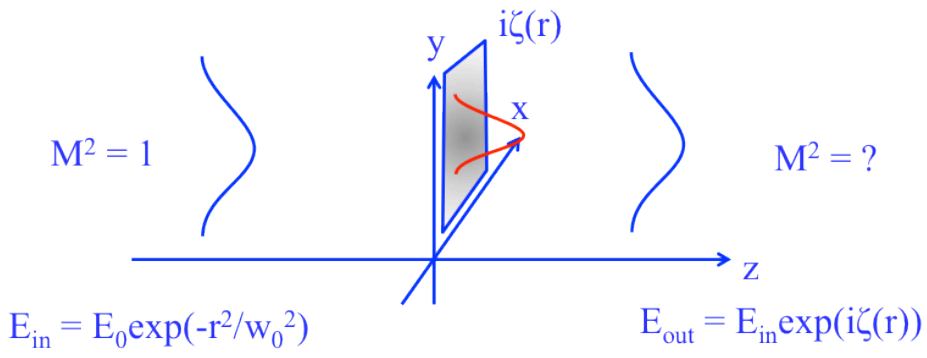

Figure 34: Geometry of modeling Gaussian beam propagation through a medium with lateral distribution of refractive index.

This problem has an analytical solution [3.9]. The M^2 of the transmitted beam is given by Eq. (3.4-3.8).

$$M_x^2 = 2k\sqrt{\langle x^2\rangle\langle\theta^2\rangle - \langle x\cdot\theta\rangle^2} \quad (3.4)$$

where

$$k\langle x\cdot\theta\rangle = -\frac{i}{P}\int xE_{out}\frac{\partial E_{out}}{\partial x}dxdy - \frac{i}{2} \quad (3.5)$$

$$\langle x^2\rangle = \frac{1}{P}\int x^2\cdot|E_{out}|^2dxdy \quad (3.6)$$

$$k^2\langle\theta^2\rangle = -\frac{1}{P}\int E_{out}\frac{\partial^2 E_{out}}{\partial x^2}dxdy \quad (3.7)$$

and

$$P = \int|E_{out}|^2dxdy \quad (3.8)$$

However, there is a challenge to create such experimental conditions that could be described by a model with reasonable complexity. Our solution is to create artificial striae that could be used for comparison between theory and experiment. (Fig. 35) shows a possible scheme of the experiment. Laser beam quality is measured after propagating through a glass sample, whose sides have all been polished, and which has a Gaussian stripe lateral refractive index profile along the y-direction, and a uniform refractive along the x and z-directions.

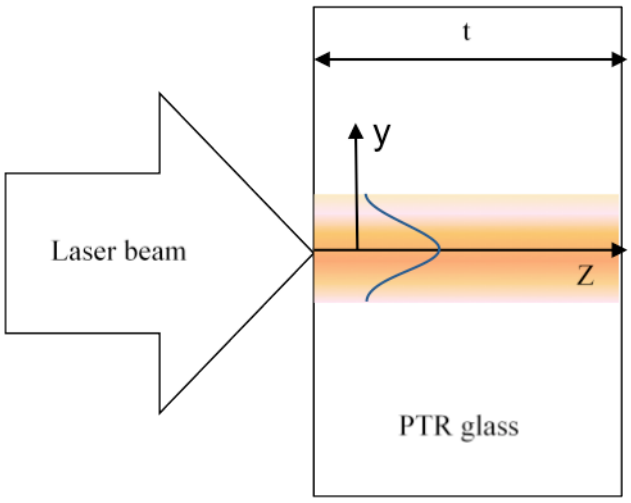

Figure 35: Artificial Gaussian stria recorded in PTR glass and directed along the laser beam propagation.

Such a stria can be fabricated in PTR glass by means of the technology depicted in (Fig 36). A plane-parallel plate of PTR glass is scanned across a beam from a He-Cd laser operating at 325 nm. This laser emits a single mode beam that has a Gaussian lateral distribution of intensity. This means that a stripe would be recorded in PTR glass with a Gaussian lateral distribution of exposure. Thus, following thermal development, this glass slab would have a stripe with a modified refractive index along the y-axis. This stripe has Gaussian distribution of refractive index along the y-axis and homogeneous refractive index profiles along the x and z-directions, (Fig. 34).

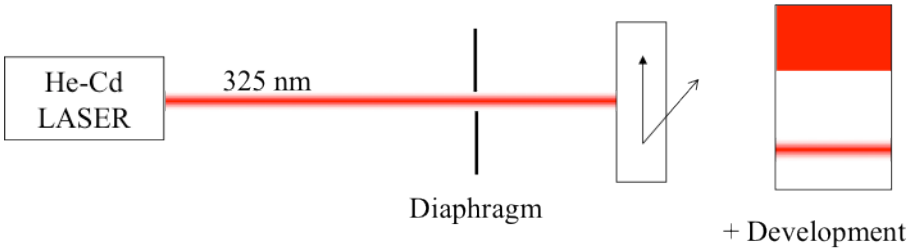

Figure 36: Method of fabrication of an artificial stria by UV exposure and thermal development in PTR glass.

The lateral profile of the refractive index recorded in the PTR glass sample is measured by a routine procedure with a shearing interferometer that is used for measurements of PTR glass photosensitivity [3.9]. Therefore, we can measure the recorded PTR samples, confirming that a lateral Gaussian refractive index profile has been recorded, and the maximum amplitude of the refractive index change (RIC) can be determined.

Several Gaussian striae were recorded with varying RIC amplitudes, these amplitudes were measured by the shearing interferometer and the resulting beam quality after propagating through the stripes was measured using the custom beam quality measurement system presented in chapter 2. The first results observed in this research are shown in (Fig. 37).

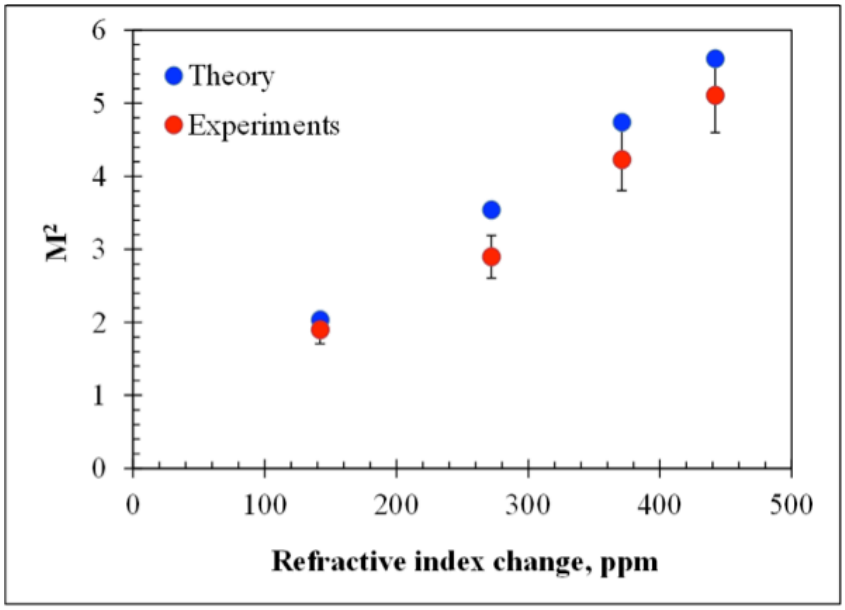

Figure 37: Dependence of beam quality (M^2) on the maximum refractive index change in Gaussian striae. Beam diameter is 2.0 mm. Striae have a lateral size of 0.55 mm, and the glass plate has a thickness of 2 mm.

It is encouraging that theoretical and experimental data are in agreement within 10%. One can see that M^2 increases almost linearly with the increase of refractive index change. From this result, we see though that the required quality of a laser beam in the range of $M^2 < 1.2$ requires extremely high optical homogeneity of an optical material placed in such an optical system, as we can see that even a Gaussian stria with a maximum RIC of only 134 ppm gives an $M^2 > 1.7$.

We also studied what is the effect of shifting the beam position in regards to this artificial stria, the results are shown in (Fig. 38). The measurement was performed on a 253 ppm Gaussian stria, once again, there is a good agreement between theory and experiment. In other words, one can see that we have developed a method that allows relating the optical homogeneity of a glass with the quality of a beam transmitted through such a glass. Based on our study, it is seen that only very small phase distortions can be allowed if we want to secure a low M^2 value of a

Gaussian beam transmitted through a non-homogeneous glass with a Gaussian distribution of refractive index, with a size comparable to the Gaussian beam.

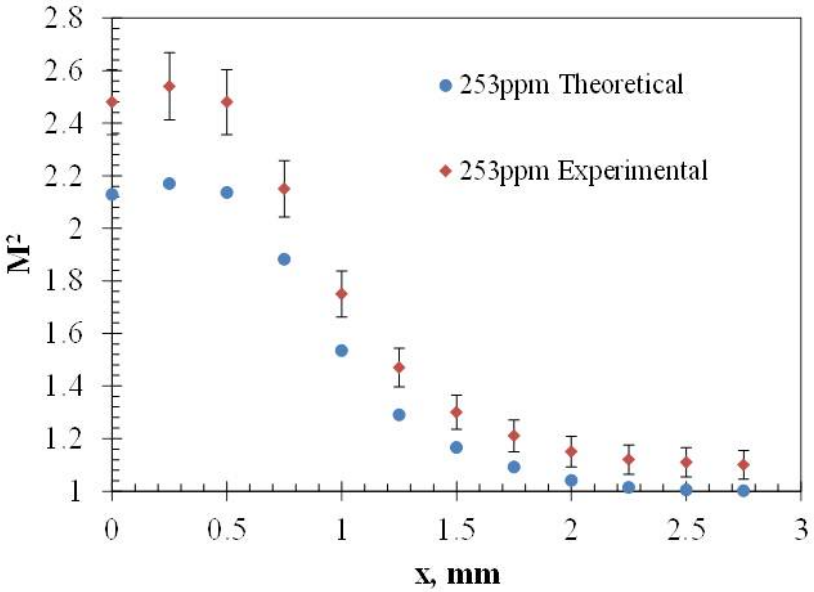

Figure 38: Dependence of beam quality (M^2) on the overlap between the illuminating beam and the Gaussian stria. Beam diameter is 2.0 mm. Stria has lateral size of 0.55 mm; amplitude of 253 ppm and glass plate has thickness of 2 mm.

In reality, requirements are high but not as high as what was demonstrated here. As a matter of fact, not only are the amplitude and the relative position of the stria to the beam important in determining the resulting beam quality, but also the shape of the stria. It turns out that a Gaussian stria illuminated by a Gaussian beam is one of the very worst configurations.

To illustrate this statement, let us understand how a stria with polynomial spatial dependence will affect the beam quality. A stria with a first order polynomial spatial dependence is equivalent to a wedge and will therefore not alter the beam quality. A similar effect is

observed when a stria has a second order polynomial spatial dependence. Whatever the amplitude of this stria, beam quality remains unchanged.

Such a result was experimentally confirmed by artificially inducing a parabolic stria in PTR and measuring the beam quality as a function of the relative position of the stria in regards to the Gaussian beam. A stria with a parabolic profile can be recorded in a PTR glass sample using the same setup to record Gaussian striae (Fig. 35); in fact the parabolic stria is simply recorded as the sum of different overlapping Gaussian lines with varying amplitudes. This parabolic stria can then be measured using the shearing interferometer, (Fig. 39) shows the results of such measurements on a parabolic stria (~ 100 ppm) recorded in a 2 mm thick sample of PTR glass.

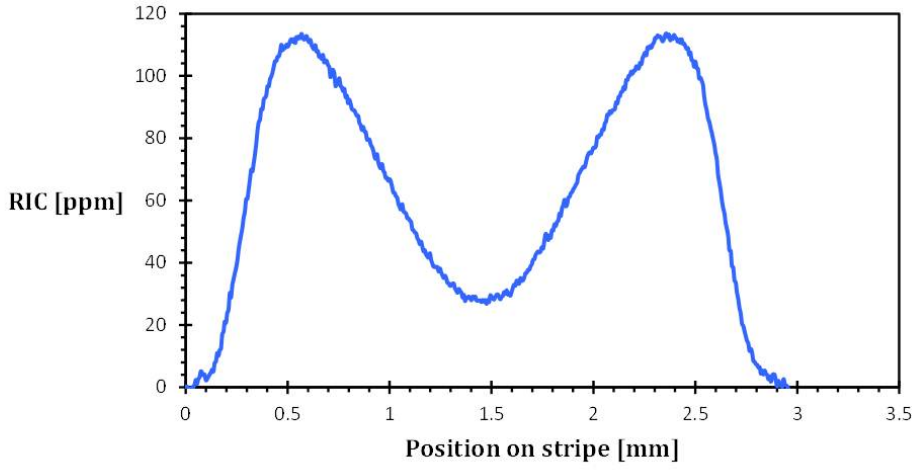

Figure 39: Parabolic stria (~100 ppm) recorded in 2 mm thick sample of PTR glass, measured by shearing interferometer.

The quality of the beam (M^2) transmitted through such a stria is then measured for various position of the stria relative to the incident Gaussian beam, (Fig. 40). We see that such a configuration has no significant effect on the quality of the beam transmitted through this stria.

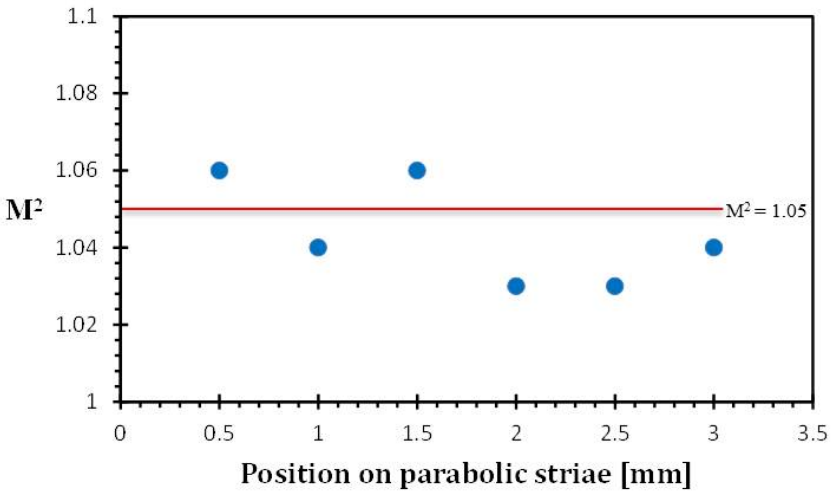

Figure 40: M^2 measurements performed on the beam transmitted through 100 ppm parabolic stria recorded in a 2 mm sample of PTR glass. Measurements are performed at various positions of the beam with respect to the stria.

This result that the beam is not deteriorated by this second order polynomial stria (parabolic stria) is not surprising, as a quadratic refractive index profile is essentially an ideal cylindrical lens. A quadratic dependent refractive index profile only acts to focus the beam without any change in the quality of the optical wavefront of the beam, even if the maximum RIC is high. In conclusion, we have seen that propagation of a Gaussian beam through a 134 ppm Gaussian stria results in an $M^2 > 1.7$ (Fig. 37), but propagation of the same beam through a quadratic refractive index profile stria with similar amplitude has no effect on the quality of the transmitted beam (Fig. 40). Therefore, what is important from these results is that

the peak-to-valley value of the refractive index fluctuations over the glass aperture is not enough to predict the beam quality after propagation through this glass and whether this glass can be used for fabricating thick CBGs.

This result is important because up to now there was no clear link between data provided by the glass community (optical homogeneity) and the data of the laser community (propagating beam quality). As of today, optical glass used for laser applications is rated on the maximum refractive index change over the glass aperture, the larger this change the worse the quality of the transmitted beam. However, as we have shown here, this maximum RIC does not provide enough information to predict the ensuing beam quality.

To overcome this lack of information, we have implemented an additional step for the characterization of PTR virgin glass blanks, used for grating recording. This step consists of measuring the quality of the beam propagating through the virgin glasses and comparing the data with the Zygo interferogram measured at 90^{o} from the beam propagation direction. (Fig. 41) shows the results on two 100 mm thick PTR glass blanks. One can see that good beam quality can be achieved after 100 mm propagation through these glasses.

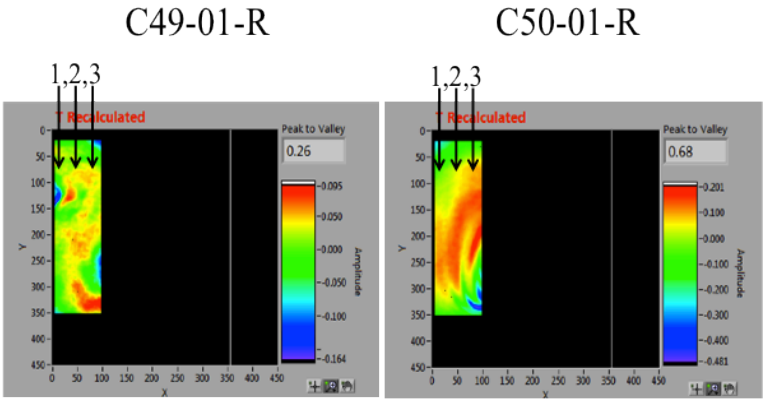

$M^2_1 = 1.1$ $M^2_1 = 1.12$
$M^2_2 = 1.11$ $M^2_2 = 1.12$
$M^2_3 = 1.11$ $M^2_3 = 1.18$

Figure 41: Zygo interferograms and corresponding M^2-value measured on two typical 100mm thick glass substrates.

This additional characterization step of virgin PTR glass blanks is critical for the fabrication of 100 mm long CBGs, where strict requirements are placed on the parameters known to distort a propagating beam, as the influence of these parameters is greater because of the large propagation distances through the optical glass.

In conclusion, we have been able to theoretically and experimentally relate glass optical homogeneity with the expected beam quality after propagation. This result therefore allows better selecting of the glasses that are used for the recording of high quality CBGs.

3.3 Beam Quality in 100 mm thick CBGs

The goal of all the previous work was for developing the tools that will permit the fabrication of CBGs with stretching times up to 1 ns, i.e. 100 mm thick CBGs. The 100 mm CBGs were fabricated at OptiGrate Corporation. The original homogeneity of the 100 mm PTR

glass samples used for recording the CBGs were optimized by implementing the characterization methods presented in this chapter, in the selection process of the PTR glass. In particular, measuring the transmitted beam quality through the 100 mm PTR samples and comparing the results with interferograms as produced by a Fizeau interferometer (Zygo Corp.), ensured that the highest quality glass was used for recording.

Figure 42: Three 100 mm thick CBGs that were fabricated at Optigrate.

Three prototype 100 mm thick CBGs were recorded in PTR glass (Fig. 42). Following fabrication and polishing, the quality of the beams diffracted by these prototypes were measured [Table 4].

Table 4: Beam Quality Measurements (M^2) of the optimized 100 mm long CBGs.

CBG/ M^2	#1	#2	#3
M^2_x	1.4	1.66	1.4
M^2_y	1.4	1.47	1.8

Along the horizontal axis of the beam, distortions are due to the original optical homogeneity as well as the photo-thermo-induced heterogeneities of the glass, these heterogeneities are known to be moderate and therefore do not severely deteriorate the quality of the beams diffracted by these CBGs along the horizontal axis. In addition, the distortions due to the optical homogeneity of the glass have been minimized (Fig. 41), as a more rigorous selection process, based on the characterization methods presented in this chapter, have been implemented in the selection of PTR glass used for recording these 100 mm CBGs.

In regards to the distortions of the diffracted beam along the vertical axis, additional effects have contributed to its deterioration, i.e. GRIN and warpage of the CBG. These distortions occur during exposure and thermal development and currently cannot be mitigated. As it was already shown, due to these two effects, the grating vectors of each section of the CBG are no longer co-linear. The different spectral components are therefore diffracted by sections of the CBGs presenting different tilt, and they therefore propagate along different directions (Fig. 31). The final diffracted beam thus presents a visible elongated shape along the vertical axis that induces an increased M^2 value.

In conclusion, our thorough investigation of the sources of distortions present in CBGs has allowed for the fabrication of100 mm thick CBGs with high beam quality between 1.35 and 1.7. Thus, we have provided the tools necessary for the fabrication of 100 mm thick CBGs with fair beam quality.

CHAPTER FOUR: STRETCHING AND COMPRESSING OF ULTRASHORT PULSES WITH CHIRPED BRAGG GRATINGS

Stretching and compressing of ultra-short pulses is accomplished via a dispersive element capable of producing a time delay between the corresponding spectral components of the pulse. This has been typically accomplished with surface gratings [4.1, 4.2], prisms [4.3], or even fiber Bragg gratings [4.4]. Recently, chirped Bragg gratings recorded in PTR glass have been shown for both stretching and compressing of ultra-short laser pulses [4.5]. These CBGs exhibit a large laser damage threshold allowing them to be implanted into high power laser systems for optical amplification of ultra-short pulses [4.6]. The ability to use the same CBG both as a stretcher and compressor makes these CBGs appealing for their compact size and robustness.

4.1 Stretching and Compressing by Chirped Bragg Gratings

One of the main points throughout this thesis has been that chirped Bragg gratings (CBGs) recorded in PTR glass are ideal candidates for stretching and re-compressing of ultra-short pulses (USPs). Let us now theoretically describe these CBGs in order to understand what makes them ideal for stretching and re-compressing USPs.

A linearly chirped Bragg grating centered at wavelength λ_0 has the following refractive index modulation along its thickness [4.7], Eq. (4.1-4.2):

$$n(z) = n_0 + n_1 \cos(Qz + \beta z^2) \qquad (4.1)$$

$$Q = \frac{4\pi n_0}{\lambda_0} \qquad (4.2)$$

Where n_0 is the average refractive index of PTR glass and n_1 is the amplitude of refractive index modulation.

$$\beta = \frac{2\pi n_0}{\lambda_0^2} \cdot \frac{\Delta\lambda}{L} \qquad (4.3)$$

For a uniform VBG the β term, Eq. (4.3) is equal to 0, while for a CBG the quadratic term βz^2 in the modulation phase Φ provides a linear longitudinal chirp of the Bragg wavelength, with Δλ the spectral bandwidth of the CBG.

It is important to note that in case of an increase of the Bragg wavelength with thickness, the β term is negative, while it only changes its sign when the Bragg wavelength decreases along the CBG's thickness. This is important, as it shows that a given delay of the group velocity dispersion after propagation and diffraction on a CBG can be fully compensated by the same CBG if used from the opposite side. In other word, a single CBG can be used for both stretching and compressing of an USP. This has already been previously demonstrated by Andrusyak et al. [4.8].

A key parameter of a CBG used for stretching and compressing USPs is the maximum stretching time that can be achieved. Stretching time is directly related to the time delay between the wavelength component that is diffracted at the front of the CBG and the wavelength component diffracted from rear of the CBG. It means that this time delay (τ) is independent of the diffracted spectral bandwidth, but only depends on the CBG's thickness, average refractive index and the speed of light, Eq. (4.4):

$$\tau = \frac{2t \cdot n_{avg}}{c} \qquad (4.4)$$

In other words, a 100 mm thick CBG is required to achieve 1 ns pulses after stretching. It is also important to stress however, that the previous equation is valid for a single diffraction on the CBG. If the same beam is diffracted from the same side of the CBG several times, the pulse duration is increased proportionally by the number of times it was diffracted. We will use this property in a further section of this chapter.

In our work a very similar approach to Andrusyak et al. [4.8] was used for stretching and re-compressing femtosecond pulses at 1.5 μm, i.e. using a single CBG, but at small incidence, typically around 5°. Using this configuration the same CBG can be used, but no polarization optics is required to separate the incident and diffracted pulse, (Fig. 43) below shows the optical configuration used in this work.

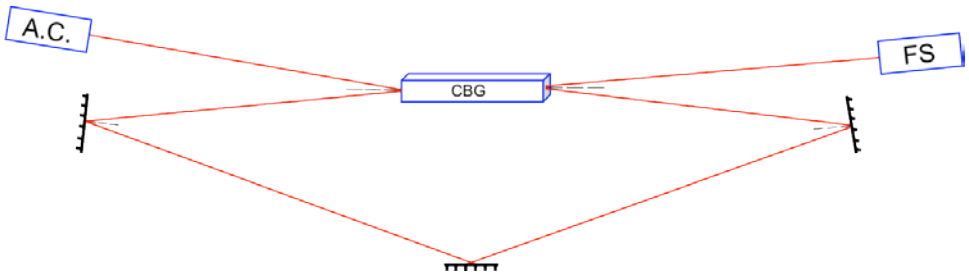

Figure 43: Scheme for stretching and compressing ultra-short pulses with a single CBG.

The light source is a femtosecond laser centered at 1552 nm. The beam is collimated using a commercial pigtailed collimator in order to produce a Gaussian beam with a 1.1 mm diameter (at $1/e^2$). The diameter of the beam was reduced in comparison with the one used for

beam quality measurements in order to minimize the effect of non-uniformity of the CBG. Because the CBG is being used at a small angle of incidence, a larger area of the CBG is probed by the incoming beam, and therefore the CBGs' non-uniformities are more likely to affect the beam after diffraction.

The beam is directed towards the CBG to be measured and diffracts on it. At this stage, the USP is stretched temporally to duration of several hundred picoseconds up to one nanosecond. Three symmetrical flat mirrors, like that shown above in (Fig. 43), are then used to redirect the beam towards the CBGs opposite face for re-compressing the USP. It is important to note that if system is perfectly aligned, the same paths occur within the CBG at stretching and compression. Thus, this configuration allows for compensation of the GVD, as all fluctuations will be seen from both sides of the CBG. After diffraction, the beam is then guided, using two steering mirrors, to the custom autocorrelator that was developed in the lab to measure the re-compressed pulse duration.

4.2 Pulse Duration Measurements

Pulse duration is one of the main parameters characterizing an USP. However, because of their extremely short temporal duration, measurement of the pulse duration cannot be achieved directly by measuring its temporal profile, as it duration is more than one order of magnitude shorter than the fastest detection system. To overcome this problem, indirect methods have been developed to measure the duration of such a pulse. Among all these methods, the autocorrelation [4.9] and the FROG [4.10] system are the most popular. In order to measure the duration of

pulses recompressed by CBGs, autocorrelation was chosen because of its simplicity to implement and because it is one of the most commonly used technique.

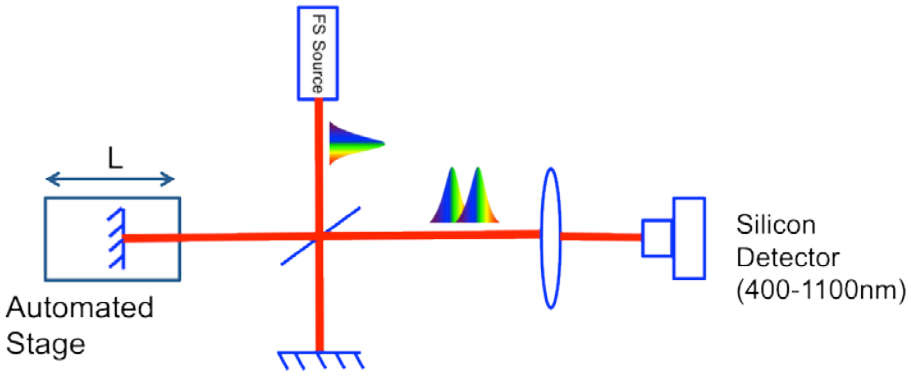

Figure 44: Autocorrelator to measure pulse duration, based on a Michelson configuration.

The system is based on a Michelson configuration (Fig. 44). The light source is a femtosecond fiber laser centered at ~1552 nm. The output beam is collimated in order to obtain a 1.1 mm beam diameter and is sent to a 50:50 beam splitter. One mirror of the interferometer is mounted and fixed to the table, while the other mirror is mounted on a Newport XPS translation stage with a resolution of 0.1 μm. We thus can adjust the position of this mobile mirror, so that its distance from the beam splitter is exactly equal to the distance of the stationary mirror from the beam splitter, ensuring that the optical path lengths of the two arms of the Michelson interferometer are identical. Then by simply moving the position of the kinematic mirror from this position of zero-path difference, we can delay one pulse in time with respect to the other. This time delay is equivalent to $2l/c$, where l is the displacement of the mirror and c is the speed of light constant. Given the resolution of our translation stage, we can control the relative delay of these pulses by as small as ~ 1.33 fs.

The beam splitter generates two individual pulses that are reflected from their corresponding mirrors, the pulses are then recombined in the beam splitter, and focused onto a ThorLabs silicon amplified detector, using a 10× microscope objective, with a NA of 0.25. Signal acquisition is performed using a National Instrument data acquisition card. Labview™ programs were developed in order to computer-control the measurements, but also in order to perform the signal processing for extracting the pulse duration.

Autocorrelation requires detecting the non-linear signal generated by the temporal and spatial overlapping of the two beams. This non-linear signal is usually obtained by a non-linear crystal that generates a second harmonic with intensity proportional to the square of the incoming intensity. For this setup, two-photon absorption of the fundamental frequency by a silicon detector was used for our autocorrelation measurements. Silicon is known not to be sensitive at 1.5 μm. However, if one focuses an ultra-short pulse on a silicon detector using a microscope objective, it becomes possible to detect a signal corresponding to two-photon absorption. However, the challenge comes from the fact that the laser source is a low energy oscillator, and thus the energy could be too low to generate two-photon absorption, even more if beam has been distorted by a CBG. To make sure that the energy of the femtosecond oscillator emitting at 1.5 μm that will be used for these experiments is high enough to produce this two photon absorption effect, the dependence of the detected signal on the distance between the detector and the focal plane of the microscope objective was measured (Fig. 45).

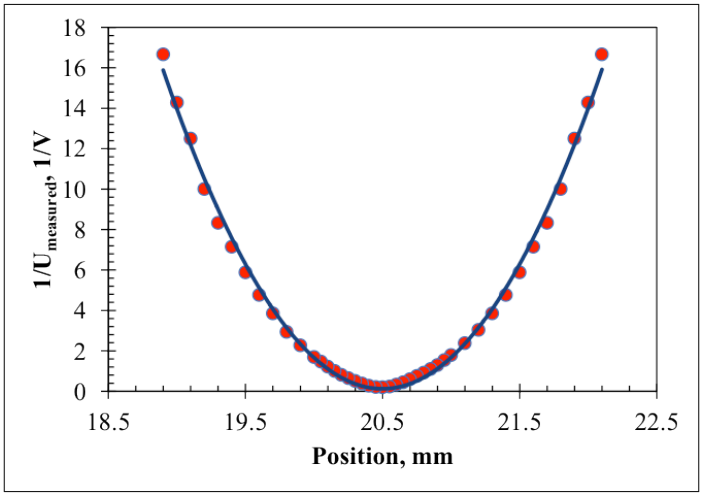

Figure 45: Dependence of the inversed detected signal on the distance between a microscope objective and a silicon detector for a constant power in the incident beam at 1.5 µm.

One can see that there is a quadratic dependence of the signal on distance while power in the beam is unchanged. This is typical for a two-photon absorption process, showing that this technique will be suitable for our measurement.

Initial measurements consisted of characterizing the duration of the pulses emitted by the femtosecond laser oscillator and processing the resulting data using LabView^{TM}. The high resolution of the translation stage allows for an interferometric autocorrelation measurement. The measurement procedure is to record a time averaged second harmonic power versus the relative delay between the identical pulses. The second harmonic power is at its highest when the pulses overlap perfectly in time and space, thus the delay between the pulses gives information regarding the duration of the pulse. The measured interferometic autocorrelation signal of the femtosecond laser used in this experiment can be seen in (Fig. 46), with the power of the signal measured in [volts] and the delay of the pulses measured in [femtoseconds].

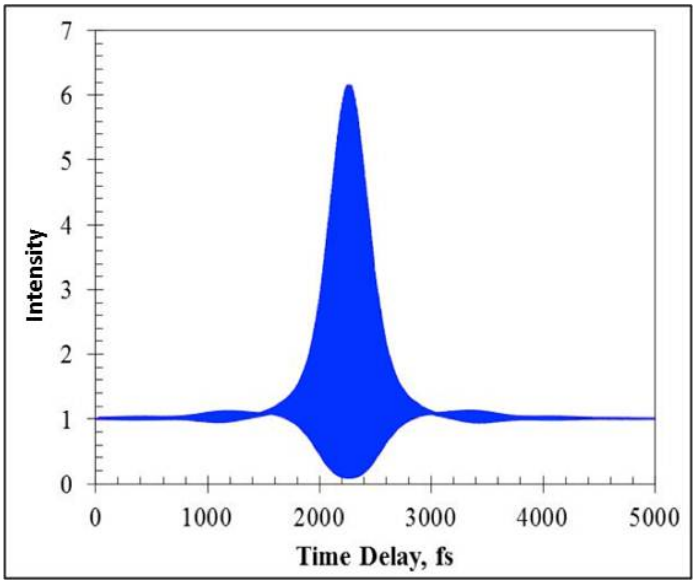

Figure 46: Result of the interferometric autocorrelation measurement on a femtosecond oscillator at 1550 nm.

The time lag delay between the pulses is related to the relative displacement of moveable mirror. This relationship comes from the additional distance *'L'* a photon has to travel to the detector which is related to time by *2L/c;* where *c* is the speed of light. The contrast ratio between the peak amplitude of the measured autocorrelation signal and the constant background level is ~ 6:1 which is in close agreement with the predicted contrast ratio of 8:1 for interferometric autocorrelation measurements. The pulse envelope (Fig. 47) was extracted from the measured interferometric autocorrelation by taking the Fourier transform of the measured signal, filtering out all components except for a small bandwidth of frequency components around DC, and taking the inverse Fourier transform of the filtered result. The temporal duration of this convolution envelope at FWHM can be related to the duration of the original pulse at FWHM by a deconvolution factor. This factor is pulse shape specific, but because the intensity

autocorrelation gives no information regarding the shape of the pulse, its shape must be assumed. For the results presented we checked whether a Gaussian or Lorentzian shape best fits the pulse shape. (Fig. 47) shows a fit of the extracted pulse envelope using a Lorentzian shape.

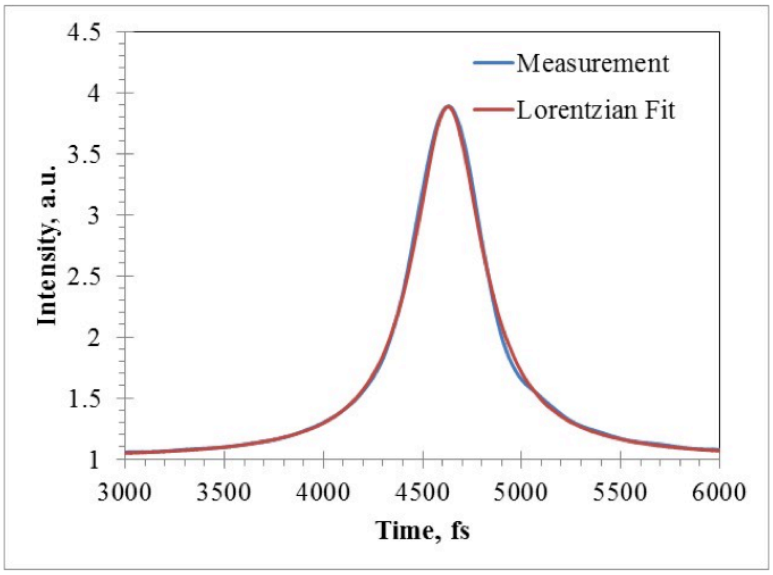

Figure 47: Pulse envelope shape and pulse duration extracted from autocorrelation measurements performed on the ultra-short pulse laser system used for characterizing stretching and compression by CBGs.

One can see that such an approximation appears reasonable. Using the Lorentzian deconvolution factor of 2.0, the measured pulse duration is calculated to be $\tau_p \approx 212$ fs at FWHM. This measurement is in good agreement with the duration of the pulse predicted from the time-bandwidth product for a transform limited Lorentzian pulse. From the given spectrum of the femtosecond laser source (Fig. 48), it can be seen that there is a bandwidth of ~7.4nm ($\Delta\lambda$) at FWHM around the central wavelength (λ_0) at 1551.4nm. From (Eq. 4.5) we can calculate the corresponding frequency bandwidth at FWHM, found to be 0.927 THz.

$$\Delta v = \frac{c^2}{\lambda_0^2}\Delta\lambda \qquad (4.5)$$

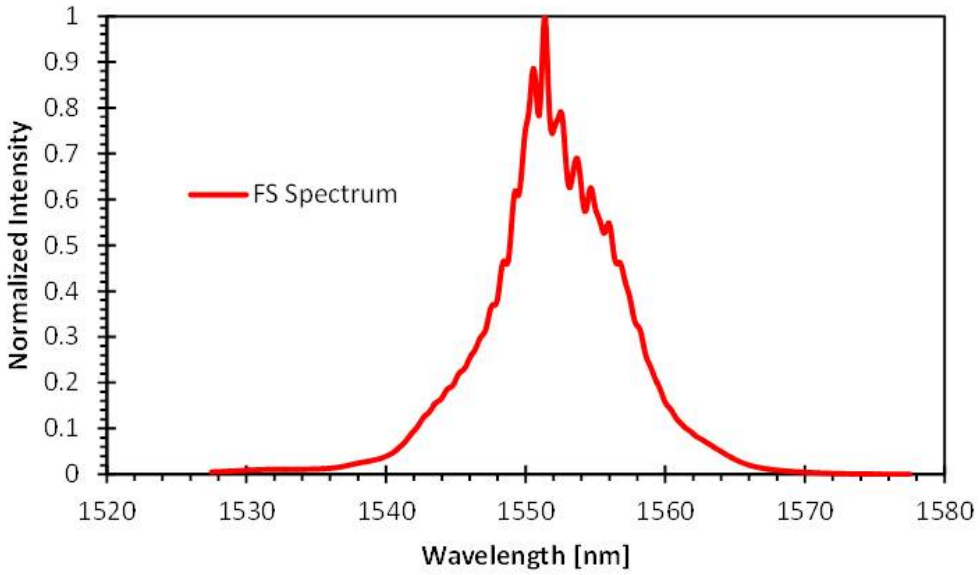

Figure 48: Spectrum of femtosecond laser at 1550nm used for stretching and compression measurements.

From the time bandwidth product for a transform limited Lorentzian pulse $\Delta\tau \bullet \Delta f = 0.142$, the pulse duration was calculated to be $\tau_{p,estimate} \approx 154.8$ fs at FWHM. Thus our measured pulse is approximately (212fs / 154.8 fs ~ 1.37) transform limited, and we see that we have developed a system for accurately measuring the duration of ultra-short laser pulses.

4.3 Correlation of Beam Quality and Re-compressed Pulse Duration

One of the goals of this work was to be able to measure the duration of a pulse after stretching and re-compressing by a CBG, and also find any possible correlation that may exist between the quality of the diffracted beam and the final pulse duration. In essence, we want to

measure the quality of the beam diffracted by the CBG and see how this correlates to the ability of the CBG to re-compress a stretched pulse to its original duration, its recompression efficiency.

This is of primary interest, as the quality of any beam will be affected after diffracting on the CBG, and because a pulse that has been stretched by a CBG will be redirected into the same CBG for recompression, An understanding of the CBG's ability to recompress a pulse whose initial beam quality is less than ideal is of considerable importance. We present here first results that demonstrate a promising trend, that the better the quality of the beam diffracted by the CBG, the better the CBG's ability to recompress the pulse to its original duration.

In order to properly perform this analysis, a large collection of data that contains both the measured beam quality of a CBG and its recompression efficiency should be collected. However, for initial testing a comparison was performed on pulses stretched and recompressed by three different 50 mm thick CBGs, centered at 1550 nm and with a 15 nm bandwidth. These CBGs were chosen for initial testing because they all had very good and similar beam quality along the horizontal axis ($M_x^2 \sim 1.15$), but they all demonstrated different beam quality along the vertical axis due to GRIN and warp in the grating.

The first CBG tested had an $M^2_y > 2.5$ and a re-compressed pulse duration measured to be 950 fs. The second CBG tested had a $M_y^2 = 1.6$ and a re-compressed pulse duration of 750 fs, while the final CBG had a $M_y^2 = 1.36$ and a re-compressed pulse duration measured to be 550fs. The results are summarized below in [Table 5].

Table 5: First results showing a correlation between the beam quality and the re-compressed pulse duration of a CBG.

	CBG #1	**CBG # 2**	**CBG # 3**
CBG	($M^2_y > 2.5$)	($M^2_y = 1.6$)	($M^2_y = 1.36$)
Pulse Duration	950 fs	750 fs	550fs

Below in (Fig. 49) we can see the improvements in the temporal pulse duration and pulse shape with improvements in beam quality. While this conclusion might be a little too early to make, it remains very encouraging that some of the problems of pulse re-compression might be sorted by improving the beam quality of the CBGs with the methods presented in this thesis.

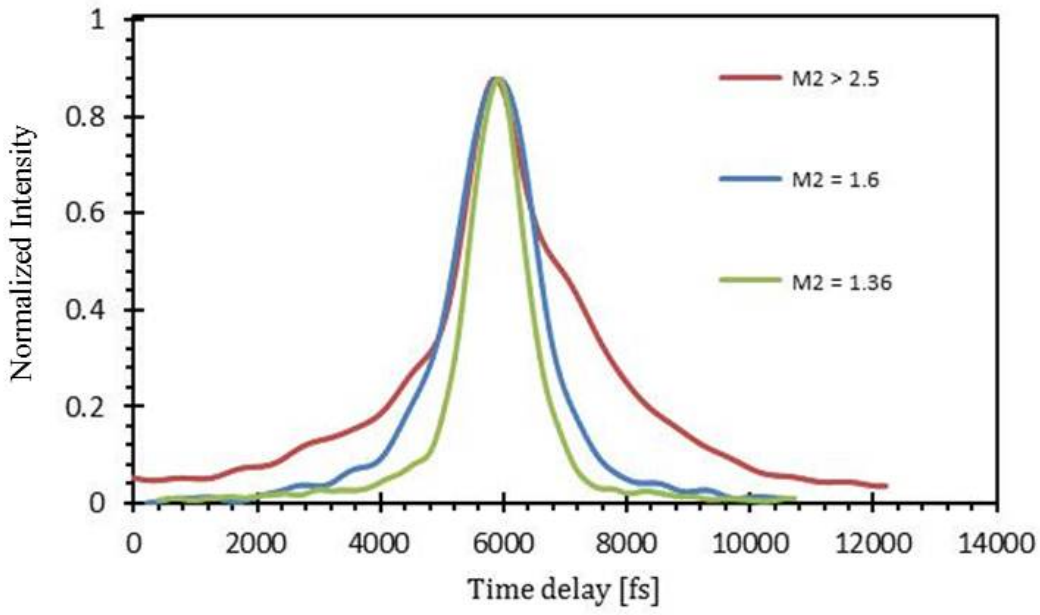

Figure 49: Improvements in recompression efficiency of CBGs as the quality of the diffracted beam is improved.

4.4. Double Pass Stretching

We have seen in a previous section that the pulse duration after stretching by a CBG is proportional to its thickness. To overcome this limitation, there were several solutions that were proposed. One of them consisted of using so-called sectional gratings. It was shown [4.10] that it is possible to replace one grating with a thickness t, a central wavelength λ_0 and a bandwidth $2\Delta\lambda$, by two gratings with thickness $t/2$, bandwidth $\Delta\lambda$, respective central wavelengths $\lambda_0-\Delta\lambda/2$ and $\lambda_0+\Delta\lambda/2$ and properly spaced in order to secure the right phase between them. While this approach is very attractive, it is very complicated to experimentally apply due to instabilities associated with maintaining the phase condition. Another approach was recently proposed [4.12], and the goal of this work consisted in testing to feasibility of this approach.

Let us consider a pulse with a spectrum which overlaps with the reflection spectral range of a CBG (Fig. 50). For a pulse propagating along the z-axis, a blue spectral component is reflected from the part of a CBG where the grating period is the shortest, while a red component is reflected from the part of CBG where the grating period is the longest. A time delay between these spectral components is thus generated.

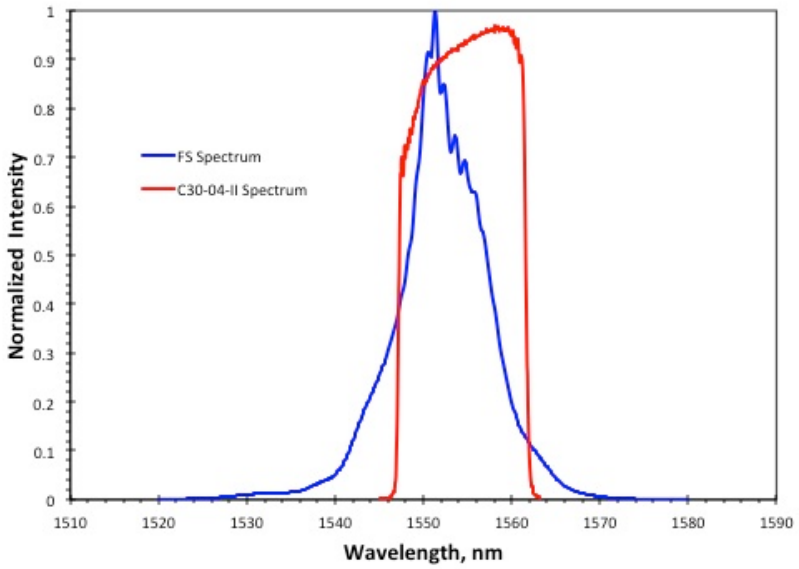

Figure 50: Spectrum of femtosecond laser at 1550nm and spectrum of CBG overlapped.

To increase the stretching time of a CBG it is possible to use multipass propagation of a laser pulse inside the CBG, this is possible by simply changing the incident angle. In this case, a pulse reflected by the CBG would not overlap with the incident pulse in space. Different spectral components would incur a lateral shift. However, this lateral shift can be compensated for if all spectral components propagate collinearly in the multipass configuration. This can be accomplished with the use of a retro-reflecting mirror. It can be external as shown in (Fig. 51), or deposited on the surface of a CBG. This configuration provides a doubling of the optical path of a laser pulse in comparison with a conventional CBG working at normal incidence. It is clear that this approach can be extended to an arbitrary number of passages to provide an optimal combination between stretching time and losses. The trajectory of a retroreflecting pulse after multiple passes finally would overlap with the trajectory of the incident pulse, therefore compensating the induced lateral shift.

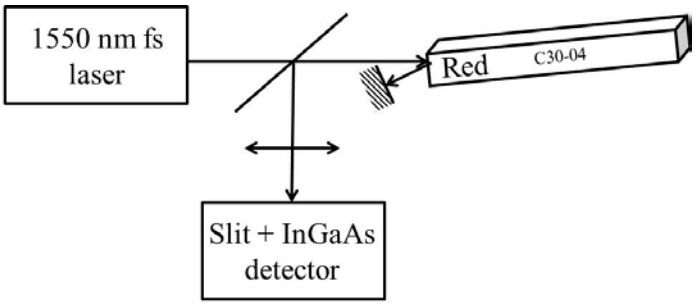

Figure 51: Double pass configuration to increase stretching time using a single CBG.

Within this work, we tested the ability to use a 50mm thick CBGs using a double pass configuration in order to stretch pulses up to 1 ns, similar to what would be obtained with a 100 mm long CBG. However, in this double pass configuration, one of the critical parameters of such a CBG is the quality of the diffracted beam after propagating 4 times through the CBG. To perform this study, we used the custom developed M^2 system to measure the quality of the beam after double stretching of the pulse. The CBG under test was provided by OptiGrate. It has a central wavelength of 1553 nm, a spectral bandwidth of about 15 nm and is 50 mm thick.

First, this CBG was tested when aligned at normal incidence (single pass configuration) in order to characterize the initial properties of the CBG. We measured the beam quality (M^2) with the beam vertically centered on the 6mm aperture of the CBG and horizontally scanned over its 10mm aperture [Table. 6]. Except close to the edge of the grating, the quality of the beam diffracted by this CBG is between 1.15 and 1.2. This result is crucial for our application, because this CBG was then horizontally tilted by ~4° such as the beam propagated over a wider CBG aperture. A flat mirror was placed at normal incidence to the diffracted beam in order to reflect it back and have it diffract for the second time on the CBG, doubling its stretching time

from 500 ps to 1 ns. The beam quality (M^2) after this double pass propagation inside the CBG was measured again across the CBG aperture. The beam quality results for the single pass and double pass configurations are both shown below in [Table. 6].

Table 6: M^2 measurements performed at different points across the aperture of the CBG for single pass and double pass configuration.

CBG	Position 1	Position 2	Position 3	Position 4	Position 5
M^2_x (Single)	1.13	1.15	1.14	1.18	1.15
M^2_x (Double)	1.43	1.34	1.37	1.47	1.46

The results show that the average beam quality measured after double pass is now ~1.4. In conclusion, the work presented in this thesis has allowed for the fabrication of quality CBGs, with good beam quality, allowing them to be used in a double pass configuration. Thus, enabling an ns-class stretcher, with good beam quality, using 50 mm thick CBGs.

CHAPTER FIVE: CONCLUSION

5.1 Thesis Summary

In this thesis a thorough investigation of CBGs recorded in PTR glass has been performed. A custom beam profiler has been developed that allows for an accurate and sensitive measurement of the transverse beam profile of a laser beam. The measurement system has been improved to allow for a SNR of 1/1000 at any point along the beam profile, as well as any position along the beam caustic. Custom coded Labview^{TM} programs have been developed to process the recorded beam profiles and calculate the corresponding M^2 value. In this thesis, this custom system has been applied to the measurement of beam quality of beams that have been diffracted by chirped Bragg gratings.

With such a sensitive measurement system, we have shown that there are several limiting parameters associated with the ISO standard M^2 measurements. First, we have shown that due to the definition of beam diameter based on the second moment of the intensity distribution, the method in which the beam profile is measured is critical, as the presence of noise or the cutting of the signal results in an over or under-estimated M^2 value. We have shown that even if proper measurement of the beam profile is carried out, the correlation between the M^2 value and the performances of such a beam in an optical system remains unclear. To overcome this problem, we proposed a new definition of beam quality coined S^2, which relies on the same measurement method but uses a different definition for the diameter of a beam. Beam diameters is defined as the size of a slit containing a given power fraction of the beam. Just as with the M^2 method, the diameter of the beam is measured according to this S^2 definition at different propagation distances after focusing the beam by a lens. Fitting this new caustic using the same equations as

used for M^2, a new beam quality metric, S^2, is obtained. Such a metric was applied for the characterization of several CBGs. We have shown that this new S^2 metric is in good agreement with M^2 for most beams but offers and insightful perspective on beams that have been deemed "poor" by the M^2 method.

Using this custom measurement system, we studied all the sources of distortions in CBGs. We first showed that PTR glass homogeneity is the first critical parameter for fabricating high quality CBGs. We developed a theoretical model and an experimental procedure in order to present a correlation between glass data (homogeneity of refractive index) and laser data (beam quality). We showed that the performance of a laser beam propagating through a heterogeneous glass can be predicted. We showed that not only the peak-to-valley value of the refractive index fluctuation over the glass aperture is critical, but also the shape of these fluctuations.

We also showed that there are other types of distortions: photo-thermo-induced distortions such as GRIN and warparge. These distortions result in the elongation of the beam after diffraction on a CBG and therefore result in a very large increase of M^2 along one direction. All this study was finally applied to the fabrication of CBGs and have allowed for the fabrication of 100°mm CBGs capable of stretching pulses to durations up to 1 ns. Both 100 mm long CBGs and 50 mm long CBGs used in double path were fabricated and their performance demonstrated.

We finally investigated the pulse duration after stretching and compression on a single CBG. We developed a custom autocorrelation system to measure the duration of these pulses and we applied it to the study of the correlation between beam quality and final pulse duration. First results showed that a correlation exists between these two parameters and therefore fabrication of distortion-free CBGs is a mandatory parameter for assembly of high throughput CPA systems.

5.2 Future Outlook

The goal of the work in this thesis was to set all the tools and methods to fabricate and characterize the performances of a CBG as a stretcher and compressor. There are still a very large number of tasks that still need to be addressed. A non-exhaustive list includes:

- From glass point of view, further improvement of glass quality is of prime interest as well as establishing new characterization methods for better selecting the glasses used for recording CBGs in PTR glass.
- From a grating point of view, it is clear that there are three main parameters that need to be better controlled in order to fabricate high quality CBGs. The first is the aberration associated with the recording beams, the second is the mitigation of GRIN and the third is the mitigation of warpage.
- From the point of view of metrology, there are two directions. The first would be to continue developing the autocorrelation system in order to benefit from its interferometric nature and extract new parameters such as the GVD of the CBG. The second critical task is to continue studying this new S^2 metric in order to demonstrate how this new metric could benefit the laser industry.
- Finally, it is clear, that there is further work associated with the use of CBGs for stretching and compressing of USPs. This includes studying the use of CBGs for longer stretching times, studying the mechanisms that degrade beam quality and re-compression efficiency, and also to study the use of tilted CBGs in combination with phase plates for temporal shaping of USP lasers.

LIST OF REFERENCES

[1.1] Oleg M. Efimov, Leonid B. Glebov, Vadim I. Smirnov, “High efficiency volume diffractive elements in photo-thermo-refractive glass,” United States Patent 6,673,497 (2004).

[1.2] O.M. Efimov, L.B. Glebov,V.I. Smirnov, L. Glebova, “Process for production of high efficiency volume diffractive elements in photo-thermo-refractive glassm,” United States Patent 6, 586, 141 (2003).

[1.3] www.OptiGrate.com

[1.4]V. Smirnov, E. Fletcher, L.B. Glebov, K. Liao, A. Galvanauskas, “Chirped bulk Bragg gratings in PTR glass for ultrashort pulse stretching and compression,” Proceedings of Solid State and Diode Lasers Technical Review, Los Angeles, SS2-1 (2005).

[1.5] M.P. Kalachnikov, V. Karpov, H. Schonnagel, W. Sander, “100-Terawatt titanium sapphire laser system,” Laser Physics, Vol. 12, 2, 368-364, (2002).

[1.6] L.B. Glebov. Volume hologram recording in inorganic glasses. Glass Science and Technology 75 C1 73-90 (2002).

[1.7] S.D. Stookey, “Photosensitive glass (a new photographic medium),” *Industrial and Engineering Chemistry*, **41**, 856-861 (1949).

[1.8] S.D. Stookey, G.H. Beall, and J.E Pierson, “Full-color photosensitive glass,” J. Appl. Phys. **49**, 5114-5123 (1978).

[1.9] J. Lumeau, L. Glebova and L. B. Glebov, "Influence of UV-exposure on the crystallization and optical properties of photo-thermo-refractive glass", Journal of Non-Crystalline Solids, **354**, 425–430 (2008).

[1.10] T. Cardinal, O. M. Efimov, H. G. Francois-Saint-Cyr, L. B. Glebov, L. N. Glebova and V. I. Smirnov, "Comparative study of photo-induced variations of X-ray diffraction and refractive index in photo-thermo-refractive glass," Journal of Non-Crystalline Solids **325,** 275 (2003)

[1.11] J. Lumeau, L. Glebova, L. B. Glebov, V. Golubkov and E. D. Zanotto, "Origin of crystallization-induced refractive index changes in photo-thermo-refractive glass," Optical Materials **32**, 139 (2009)

[1.12] O. M. Efimov, L. B. Glebov and V.I. Smirnov. Diffractive optical elements in photosensitive inorganic glasses. Inorganic Optical Materials III A.J. Marker, M.J. Davis, Editors. Proceedings of SPIE, v. 4452 (2001) 39-47.

[1.13] L.Glebov, “Volume Bragg Gratings in PTR Glass--New Optical Elements for Laser Design,” 3rd Advanced Solid-State Photonics (ASSP) Topical Meeting. ASSP Technical Digest, Paper Code MD1, Nara, Japan, January 2008.

[1.14] L.Glebov, “High brightness laser design based on volume Bragg gratings,” Laser Source and System Technology for Defense and Security II. Proceedings of SPIE 6216 (2006) 621601.

[1.15] A.Sevian, O.Andrusyak, I.Ciapurin, G.Venus, V.Smirnov, and L.Glebov, "Efficient Power Scaling of Laser Radiation by Spectral Beam Combining," Opt. Lett. 33 (2008) 384-386.

[1.16] O.Andrusyak, V.Smirnov, G.Venus, V.Rotar, and L.Glebov, "Spectral Combining and Coherent Coupling of Lasers by Volume Bragg Gratings," IEEE Journal of Selected Topics in Quantum Electronics, 15 (2009) 344-353.

[1.17] J. Lumeau, L. Glebova and L. B. Glebov, "Near-IR absorption in high purity photo-thermo-refractive glass and holographic optical elements: measurement and application for high energy lasers", Applied Optics **50**(30), 5905–5911 (2011)

[1.18] L. Glebova, V. Smirnov, J. Lumeau, L. Glebov, "Low losses volume Bragg gratings recorded in photo-thermo-refractive glass", Photonics West (San Francisco, California, USA), paper 8257-44 January 2012

[1.19] Brian Anderson ; Sergiy Kaim ; George Venus ; Julien Lumeau ; Vadim Smirnov, Boris Zeldovich and Leonid B. Glebov, "Forced air cooling of volume Bragg gratings for spectral beam combination," Proc. SPIE 8601, Fiber Lasers X: Technology, Systems, and Applications, 86013D (2013);

[1.20] D. Strickland and G. Mourou, "Compression of amplified chirped optical pulses," Optics Communications **56**, 219 (1985)

[1.21] M. D. Perry, D. Pennington, B. C. Stuart, G. Tietbohl, J. A. Britten, C. Brown, S. Herman, B. Golick, M. Kartz, J. Miller, H. T. Powell, M. Vergino, and V. Yanovsky, "Petawatt laser pulses," Opt. Lett. 24, 160-162 (1999)

[1.22] A. Boskovic, M. J. Guy, S. V. Chernikov, J. R. Taylor, and R. Kashyap, "All-fibre diode pumped, femtosecond chirped pulse amplification system," Electron. Lett. **31**, 877 (1995)

[1.23] A. Galvanauskas, M. E. Fermann, D. Harter, K. Sugden, and I. Bennion, "All-fiber femtosecond pulse amplification circuit using chirped Bragg gratings," Appl. Phys. Lett. **66**, 1053 (1995)

[1.24] L. B. Glebov, E. Flecher, V. I. Smirnov, A. Galvanauskas, K. Liao, "Stretching and compression of laser pulses by means of high efficiency volume diffractive gratings with

variable periods in photo-thermo-refractive glass," United States Patent **7,424,185 B2** (2008)

[1.25] Oleg M. Efimov, Leonid B. Glebov, Larissa N. Glebova, Kathleen C. Richardson, and Vadim I. Smirnov, "High-Efficiency Bragg Gratings in Photothermorefractive Glass," Appl. Opt. 38, 619-627 (1999)

[1.26]Petermann, E.I., Skaar, J., Sahlgren, B.E., Stubbe, R.A.H., Friberg, A.T., "Characterization of fiber Bragg gratings by use of optical coherence-domain reflectometry, " Journal of Lightwave Technology 17(11) (1999)

[1.27] V. Smirnov, E. Flecher, L. Glebov, K-H. Liao and A. Galvanauskas, "Chirped bulk Bragg gratings in PTR glass for ultrashort pulse stretching and compression," SSDLTR, Los Angeles, 2005, SS2-1

[1.28] Guoqing Chang, Matthew Rever, Vadim Smirnov, Leonid Glebov, and Almantas Galvanauskas, "Femtosecond Yb-fiber chirped-pulse-amplification system based on chirped-volume Bragg gratings," Opt. Lett. 34, 2952-2954 (2009)

[2.1] Anthony E. Siegman, "Defining, measuring, and optimizing laser beam quality", Proc. SPIE 1868, Laser Resonators and Coherent Optics: Modeling, Technology, and Applications, 2 (1993).

[2.2] Shojiro Nemoto, "Determination of waist parameters of a Gaussian beam," Appl. Opt. 25, 3859-3863 (1986)

[2.3] Russell L. McCally, "Measurement of Gaussian beam parameters," Appl. Opt. 23, 2227-2227 (1984)

[2.4] H. Weber, "Some historical and technical aspects of beam quality," Opt. Quantum Electron. 24, S861-S864 (September 1992).

[2.5] ISO Standard 11146, "Lasers and laser-related equipment – Test methods for laser beam widths, divergence angles and beam propagation ratios" (2005)

[2.6] C. B. Roundy, "Current Technology of Laser Beam Profile measurements," tutorial from the Spiricon website

[2.7] Slater, John M., and Brian Edwards. "Characterization of highpower lasers." Laser Technology for Defense and Security VI. Ed. Mark Dubinskii & Stephen G. Post. Orlando, Florida, USA: SPIE 76860W-12 (2010).

[2.8] http://www.ophiropt.com/laser-measurement-instruments/beam-profilers/products/camera-based-profilers/m2-1780

[2.9] T, Sean Ross, William P. Latham, Appropriate Measures and Consistent Standard for High Energy laser Beam Quality, Journal of Directed Energy Vol. 2, Number 1, PP. 22-58 (2006)

[3.1] K. Liao, C. Liu, A. Galvanauskas, E. Flecher, V. Smirnov, and L. Glebov, "A novel chirped pulse amplification system based on a monolithic large aperture bulk-Bragg-grating stretcher/compressor," in Advanced Solid-State Photonics (TOPS), C. Denman and I. Sorokina, eds., Vol. 98 of OSA Trends in Optics and Photonics (Optical Society of America, 2005), paper 768.

[3.2] K. Liao, M. Cheng, E. Flecher, V. Smirnov, L. Glebov, and A. Galvanauskas, "Large-aperture chirped volume Bragg grating based fiber CPA system," Opt. Express 15, 4876-4882 (2007).

[3.3] Christophe Moser ; Frank Havermeyer; Distortion free pulse stretching and compression by chirped volume holographic gratings. Proc. SPIE 7581, High Energy/Average Power Lasers and Intense Beam Applications IV, 75810E (February 17, 2010); doi:10.1117/12.842706.

[3.4] Sergiy Mokhov, Vadim Smirnov, Eugeniu V. Rotari, Julien Lumeau, Boris Y. Zeldovich, Leonid B. Glebov, “Deterioration of beam quality factor of laser pulses due to angular dispersion of optical elements”, Proc. of Photonics West, Paper 8603-3 (2013).

[3.5] J. Lumeau and L.B. Glebov, “Gradient of induced refractive index effect in photo-thermo-refractive glass”, Conference on the Physics of Non-Crystalline Solids, paper M134 (2013).

[3.6] APPLE Phase I project reports (2008-2009).

[3.7] Schott Technical information, TIE-26: Homogeneity of optical glass (http://www.schott.com/advanced_optics/english/community/technical-papers-and-tools/tie.html?so=france&lang=french)

[3.8] Sergiy Mokhov, Derrek Drachenberg, Ivan Divliansky, George Venus, Boris Zeldovich, and Leonid Glebov, “Modeling of High-Power Spectral Beam Combining with Thermally Distorted Volume Bragg Gratings”, Photonics West LASE, 7915 − High Energy/Average Power Lasers and Intense Beam Applications VI, paper 7915-17

[3.9] .M. Efimov, L.B. Glebov, H.P. Andre. Measurement of the induced refractive index in a photothermorefractive glass by a liquid-cell shearing interferometer. Appl. Optics, 41 1864-1871 (2002)

[4.1] Treacy, Edmond. "Optical pulse compression with diffraction gratings." *Quantum Electronics, IEEE Journal of* 5.9 (1969): 454-458.

[4.2] Cheriaux, G., et al. "Aberration-free stretcher design for ultrashort-pulse amplification." *Optics letters* 21.6 (1996): 414-416.

[4.3] Akturk, Selcuk, et al. "Extremely simple single-prism ultrashort-pulse compressor." *Opt. Express* 14.21 (2006): 10101-10108.

[4.4] Eggleton, Benjamin J., et al. "Experimental demonstration of compression of dispersed optical pulses by reflection from self-chirped optical fiber Bragg gratings." *Optics letters* 19.12 (1994): 877-879.

[4.5] Galvanauskas, Almantas, and Martin E. Fermann. "Optical pulse amplification using chirped Bragg gratings." U.S. Patent No. 5,499,134. 12 Mar. 1996.

[4.6] Efimov, Oleg M., et al. "Laser-induced damage of photo-thermo-refractive glasses for optical holographic element writing." *Laser-Induced Damage in Optical Materials: 1998*. International Society for Optics and Photonics, 1999.

[4.7] Sergiy Mokhov, Christopher Lantigua, Julien Lumeau, Vadim Smirnov, Boris Y. Zeldovich, Leonid Glebov, "Characterization of optical elements by beam quality deterioration," SPIE Optical Metrology Meeting, Paper 8789-31 (2013)

[4.8] Oleksiy Andrusyak, Lionel Canioni, Ion Cohanoschi, Eugeniu Rotari, Vadim Smirnov, George Venus, and Leonid Glebov, "Cross-correlation technique for dispersion characterization of chirped volume Bragg gratings," Appl. Opt. 48, 5786-5792 (2009)

[4.9] J. A. Armstrong, "Measurement of picosecond laser pulse widths," Appl. Phys. Lett. 10, 16 (1967)

[4.10] Daniel J. Kane and Rick Trebino, "Single-shot measurement of the intensity and phase of an arbitrary ultrashort pulse by using frequency-resolved optical gating," Opt. Lett. 18, 823-825 (1993).

[4.11] Andrusyak, Oleksiy; Canioni, Lionel; Cohanoshi, Ion; Delaigue, Martin; Rotari, Eugeniu; Smirnov, Vadim; Glebov, Leonid, "Sectional chirped volume Bragg grating compressors for high-power chirped-pulse amplification," Solid State Lasers XIX: Technology and Devices. Edited by Clarkson, W. Andrew; Hodgson, Norman; Shori, Ramesh K. Proceedings of the SPIE, Volume 7578, article id. 75781A, 11 pp. (2010).

[4.12] O. Andrusyak, Almantas Galvanauskas, l. Glebova, L. B. Glebov, J. Lumeau, S. Mokhov, V. Smirnov, B. Ya. Zeldovich, "Laser pulse temporal, spectral and spatial shaping devices based of volume diffractive gratings with spatially variable parameters", *Patent pending*, Application # **61/294,566**, March 2009.